A MODERN SURVEY AND HOLOCENE RECORD OF LAKE WATER AND DIATOM ISOTOPES FROM SOUTH ALASKA

By Caleb J. Schiff

A Thesis

Submitted in Partial Fulfillment

of the Requirements for the Degree of

Master of Science

in Geology

Northern Arizona University

December 2007

Approved:

Darrell Kaufman, Ph.D., Chair

R. Scott Anderson, Ph.D.

Mary Reid, Ph.D.

Al Werner, Ph.D.

ABSTRACT

A MODERN SURVEY AND HOLOCENE RECORD OF LAKE WATER AND DIATOM ISOTOPES FROM SOUTH ALASKA

CALEB SCHIFF

Oxygen isotopes of diatoms ($\delta^{18}O_{diatom}$) record the isotopic composition of lake water (δW) in lakes of maritime south Alaska and provide insights into past changes in atmospheric circulation. Lake water and sediment were collected along an elevational transect in south Alaska and analyzed for paleoclimate studies. δW and climate data show a strong gradient from maritime to interior sites. In general, δW from coastal lakes reflect the isotope composition of local precipitation (δP) and define the local meteoric water line (LMWL), which is parallel to the global meteoric water line. δW from interior lakes, however, are influenced by evaporation and exhibit a lower slope (6 versus 8). $\delta^{18}O_{diatom}$ from modern sediments show a strong correlation with δW ($r = 0.99$) and local mean annual air temperature ($r = 0.94$). The modern spatial relationships cannot be explained by temperature-dependent fractionation effects alone, nor by physiographic characteristics of the lakes (e.g., lake and watershed area), so cannot be used for quantitative paleotemperature reconstructions. These analyses reaffirm the complexity of North Pacific δP and the secondary role of temperature on δW values in the region. The paucity of δP data from south Alaska further hampers paleotemperature

reconstructions. Changing wintertime moisture source is the most probable control on regional δP, which is strongly linked to the intensity and position of the Aleutian Low (AL).

Sediment cores were recovered from Mica Lake (60.96° N, 148.15° W; 100 meters above sea level), an evaporative-insensitive lake in the western Prince William Sound. The lake sediment contains massive gyttja, sand-rich avalanche deposits, and six tephra deposits. Thirteen calibrated ages on terrestrial and macrofossil samples were used to construct an age-depth model for core MC-2 and suggests that the core spans the last 9910 yr. The average sedimentation rate from the age model is 0.30 mm/yr and the average uncertainty based on the 95% confidence interval is ± 112 yr. Half-cm-thick samples, representing ~15 yr of sedimentation, were sampled at different intervals from core MC-2. Contiguous magnetic susceptibility measurements helped identify tephra deposits. Percent organic matter (OM) and biogenic silica (BSi) record lake productivity. OM and BSi have a first-order increase between 9.6 ka and 2.5 ka, then descreases towards 0.1 ka and covary (r = 0.52).

Diatoms from 46, 0.5-cm-thick samples were isolated and analyzed for their oxygen isotope ratios. The analyses employed a newly designed, stepwise fluorination technique, which uses a CO_2 laser-ablation system, coupled to a mass spectrometer. $\delta^{18}O_{diatom}$ values range between 25.2 and 29.8‰ and have a reproducibility of 0.2‰. $\delta^{18}O_{diatom}$ values are relatively uniform between 9.6 and 2.5 ka, but exhibit a four-fold increase in variability since 2.5 ka. The 20th century shows a 4.6‰ increase of $\delta^{18}O_{diatom}$. Late Holocene excursions to lower $\delta^{18}O_{diatom}$

values suggest a more western or southwestern moisture source (Bering Sea) delivered by zonal flow, while higher $\delta^{18}O_{diatom}$ values reflect more southern moisture (Gulf of Alaska), delivered by meridional flow. Zonal flow likely corresponds to weaker AL because the south-to-north storm track is less prominent, allowing moisture from the west to reach south Alaska. Comparisons with regional δP records support the moisture-source hypothesis and also document late Holocene atmospheric instability.

This study is the first detailed investigation of δW from south Alaska. The results provide a more complete understanding δW in south Alaska to be applied to future paleoclimate studies from the region.

ACKNOWLEDGEMENTS

While intelligence and stubbornness has often helped me reach many achievements in my life, completing this thesis required perpetual motivation. I thank my advisor, Darrell Kaufman, for continued encouragement during the past two years. Darrell is the definition of a great advisor: his attention to detail, rapid turnover of drafts and emails, and his ability to sense his students extent of "burn-out" helped me immensely, especially during this last semester. Completing this thesis would not have been possible without his dedication to me and our research.

I thank my field assistants, Nick McKay, Tom Daigle, Chris Kassel, Eric Helfrich, and Peggy Foletta for their hard work in often less-than ideal south Alaska conditions. Our time spent playing *Set-back* and sharing glasses of "Killer-Juice" after long days at Mica Lake will not be forgotten. Kristi Wallace provided invaluable assistance in Anchorage and her hospitality and excellent food recharged the field crew for continued field work. Kristi also advanced my understanding of local tephra records and provided important geochemical data of tephra from Mica Lake.

I thank Andrew Henderson for teaching me the finer points of diatom isolation. Mastering the sensitive procedure was a necessity for success of this thesis.

I thank Justin Dodd for his work towards refining the diatom analyses using the laser-ablation mass spectrometer. It was exciting to develop the new methodology that has advanced this research.

I thank Rick Doucett for his extra effort towards analyzing water isotopes from my south Alaska collections.

I thank Ryan Vachon who guided and advised me through my early undergraduate years at the University of Colorado. Ryan inspired and helped me to pursue science while living life to its fullest, which is a balance I often struggle to find. I also (jokingly) blame Ryan for sparking my interest in studying the stable isotopes of precipitation, which can leave anyone feeling perplexed, frustrated, and ready for a beer at the end of the day!

I thank my family and friends for being patient during the last two years. Although I know they enjoy hearing stories and viewing pictures of research in Alaska, my commitment to research requires me to spend less time with loved ones and I am grateful for their understanding.

During the last five months, at home, work, and in the field, Heidi Roop has added a new, exciting, and fulfilling dimension to my life. I am grateful for her patience, warm meals, and attentive listening during stressful times. Warm *Mochis* and afternoon coffee dates go a long way. I look forward to providing similar love and support for her as she pursues her Master's degree with Darrell.

I thank the Geological Society of America's Limnology and Quaternary and Geomorphology divisions for their support and awards. Recognition by these two groups help me stay motivated and reaffirmed the quality of my work.

Funding for this research was provided by the National Science Foundation (NSF: ARC-0455043), the US Geological Survey, the Geological Society of America, and the Friday Lunch Clubbe.

TABLE OF CONTENTS

Page

List of Tables

Page

List of Figures

Page

1. Introduction

Lake water isotopes (δW) integrate spatial and temporal changes in climate on a variety of scales. For lakes with long water residence times, δW often varies with the precipitation/evaporation balance (E/P), whereas δW in lakes with short residence times more directly reflect the isotopic composition of precipitation (δP). Empirical observations during the last ~50 years demonstrate the strong spatial and temporal relationship between δP and environmental parameters (Dansgaard, 1964; Rozanski et al., 1993). Perhaps most notable is the correlation between δP values and latitude, with lower values towards the poles. However, departures from the general poleward depletion are apparent from more detailed investigations of modern and paleorecords of δP (e.g., Yurtsever and Gat, 1981; Boyle, 1997). Specifically, large-scale vapor transport can change the origin and moisture pathway, which cause different amounts of fractionation for a given site and latitude (Bowen and Wilkinson, 2002). Because there are multiple controls on δP, unambiguous climate interpretations are difficult without a more complete understanding of regional effects on δP. Calibration between δP and climate can sometimes be obtained from long-term site collections, but these data are sparse. Surveys of modern δW of a region may be the best method to disentangle the spatial and temporal variability of δP because lakes are spatially dense in some regions and provide 'averaged' conditions, which are most practical for paleoclimate interpretations.

Numerous components of lake sediments have been investigated for records of δW, including: chironomid head capsules (e.g., Wooller et al., 2004; in prep.),

aquatic cellulose (e.g., Abbott et al., 2000; Sauer et al., 2001), and authigenic carbonate (e.g., Abell and Hoelzmann, 2000; Hu et al., 2001; Anderson et al., 2005). No one component is a panacea because of individual shortcomings. For example, authigenic carbonate studies are limited to alkaline lakes and aquatic cellulose may not be continuously preserved (e.g., Sauer et al., 2001). Also, non-climate controls must be considered when using biogenic material because fractionation occurs during formation, although laboratory and field studies provide good estimates of the magnitude of fractionation effects during the transfer of isotopes from water to sediment (e.g., Sauer et al., 2001; Moshen et al., 2005). Most recently, the oxygen isotopes of lake diatoms ($\delta^{18}O_{diatom}$) have emerged as an alternate proxy of paleo δW (see review in Leng and Barker, 2006). Diatoms are ubiquitous in most lakes and their silica structure ensures good preservation. Recent advances in diatom separation techniques (Rings et al., 2004) and mass spectrometry (Dodd et al., in press) have expanded the method to lakes with relatively low productivity. Studies of $\delta^{18}O_{diatom}$ have been used as a record of temperature (e.g., Shemesh and Peteet, 1998; Hu and Shemesh, 2003), δP (e.g., Shemesh et al., 2001; Rosqvist et al., 2004), and lake E/P (e.g., Lamb et al., 2005).

In this study, I investigate the oxygen isotope composition of water and diatoms recovered from south Alaskan lakes and their respective watersheds. My investigations reveal large spatial and temporal variability of δW and $\delta^{18}O_{diatom}$. The modern δW data span three climate regimes and the $\delta^{18}O_{diatom}$ temporal record from one site extends to 9600 yr BP. The modern distribution of δW clearly demonstrates that maritime δW reflects δP, whereas interior lakes are strongly affected by

evaporation. The current understanding of δP in the North Pacific region does not allow a simple interpretation of the 9600 yr $\delta^{18}O_{diatom}$ record but multiple controls are considered. I suggest that δP in south Alaska is strongly dictated by the moisture source and therefore changing δW is driven by large-scale changes of North Pacific atmospheric circulation. Specifically, the strength and position of the Aleutian Low (AL) is suggested as the main control of δP in south Alaska.

2. Background

2.1. Stable isotopes of precipitation

A global survey of the isotopes of precipitation (δP), now operated by the International Atomic Energy Agency's Global Network for Isotopes in Precipitation (IAEA-GNIP), began in the 1960's in an effort to better understand the spatial and temporal variability of δP and their link to climate. Empirical relationships between δP and environmental parameters at collection stations (e.g., air temperature, amount of precipitation, altitude, distance to coast) are well documented (Dansgaard, 1964; Yurtsever and Gat, 1981; Rozanski et al., 1993; Araguás-Araguás et al., 2000). In general, local relationships observed between δP and environmental parameters described the amount of "rain-out" of moisture from its source due to preferential loss of heavier isotopes (^{18}O, D) (Dansgaard, 1964). Statistical analyses of the global data set show that δP is most strongly correlated with average monthly temperature; latitude, altitude, and amount of precipitation are of lesser importance (Yurtsever and Gat, 1981). In addition to the amount of rain-out, δP is affected by moisture source

conditions (e.g., sea surface temperature, humidity, and windiness). The IAEA-GNIP program has continued routine collections to add to this database, which presently includes over 250,000 collections (Araguás-Araguás et al., 2000). Only 9% of collections are from sites above 60° latitude, however, and data from network stations often have long gaps between collections. Thus, many areas of the globe lack robust records of δP, hindering paleoclimate studies that use oxygen and hydrogen isotopes in geologic archives. Interpolation and modeling of modern δP and meteorological data has provided a more complete map of the spatial distribution of δP (Bowen and Wilkinson, 2002). These maps highlight areas for future monitoring and regions where large-scale vapor transport pathways prevent accurate interpolation between IAEA-GNIP stations. Models are used to interpret records of δP and the mechanisms that cause δP to vary in areas with little data (Bowen and Wilkinson, 2002; Kavanaugh and Cuffey, 2003; Bowen and Ravenaugh, 2003; Fisher et al., 2004).

Biogenic and abiotic minerals that precipitate in lake and marine water and are preserved in deposits are archives of δW, but the influence of a wide range of environmental variables prevents simple interpretations. By combining baseline conditions (e.g., modern δP and δW distributions and meteorological data) with an understanding of the formation effects on any particular archive, the relationship between δP, δW, and a sediment record can be disentangled. Using records of δW as a paleothermometer is common, although the influence of changes in location or conditions of the moisture source are well documented in ice cores (e.g., Boyle et al.,

1997; Masson-Delmotte et al., 2005; Stenni et al., 2001), speleothems (e.g., Denniston et al., 1999), and lake sediment (e.g., Rosqvist et al., 2004).

2.2. North Pacific climate variability and δP records

Climate variability in the North Pacific is associated with large-scale, interannual (e.g., El Niño-Southern Oscillation [ENSO]) and interdecadal (e.g., Pacific Decadal Oscillation [PDO]) climate oscillations (Trenberth and Hurrell, 1994; Papineau, 2001; Moore et al., 2003). The PDO is often viewed as ENSO-like phenomena associated with interdecadal climate variability because of their similar spatial patterns (e.g., Mantua et al., 1997). In south Alaska, winter surface air temperature and precipitation are largely determined by the strength and position of the Aleutian Low (AL), a low-pressure system that steers wintertime storms inland to south Alaska (Fig. 1a) (Rodionov et al., 2005). The AL has no observed influence on summer conditions. The DJF North Pacific Index (NPI), calculated as the area-weighted, sea-level pressure over the region 30°N-65°N, 160°E-140°W (Trenberth and Hurrell, 1994), provides a measure of the intensity of the wintertime AL (Fig. 2). Negative NPI is associated with a strong AL. The interdecadal variability of the AL is clearly seen when a 15 yr moving average is calculated from the annual DJF NPI (Fig. 2). Strong shifts of the NPI have occurred three times during the 20th century, centered at 1925, 1947, and 1977.

Modern and paleoclimate records of the AL have provided an understanding of its direct regional influence. Rodionov et al. (2005) reviewed the meteorological expression of the 10 strongest and weakest AL years between 1951 and 2000 in the

North Pacific (Fig. 1a; Table 1). The AL is split into two centers during weak years, one in the Gulf of Alaska and one east of Kamchatka. In the Gulf of Alaska, storms come from the west and northwest during weak AL years and from the southwest during strong AL years. The increased southerly flow into the Gulf of Alaska brings warm, moist air inland to south Alaska, which is well recorded at climate stations in south-central Alaska (Fig. 1b). Inverse (cold and dry) conditions occur farther west in the Aleutian Islands during strong AL years. Farther north at Anchorage, recorded precipitation does not show much increase but average temperatures are 5 °C warmer during strong AL years (Fig. 1b).

The AL's link to storm intensity in the North Pacific (Trenberth and Hurrell, 1994; Rupper et al., 2004), its decadal variability during the 20th century (Overland et al., 1999), and its predicted intensification and northward shift under global warming (Yin, 2005; Salathé, 2006) is motivation to reconstruct the AL beyond historical time periods. South Alaska is located along the North Pacific storm track and is therefore an ideal location to record variability of the AL. Terrestrial climate records from this area are strongly influenced by the AL. The mass balance of glaciers (e.g., Hodge et al., 1998), organic matter in lake sediments (e.g., McKay, 2007), increases in far-traveled pollen (Spooner et al., 2003), the accumulation rate in ice cores from Mt. Logan (Rupper et al., 2004), and the effective moisture in interior Yukon (Anderson et al., 2005) have been interpreted as variability in the AL on decadal to millennial time scales.

Paleo-δP records from the North Pacific region suggest that air temperature is not the primary control on δP (e.g., Wake et al., 2002; Fisher et al., 2004; Anderson

et al., 2005). For example, δP data from Mt. Logan ice cores do not correlate significantly with instrumental or paleotemperature records (Holdsworth et al., 1992; Wake et al., 2002). Significant deviation between temperature-driven isotope models and modern δP from IAEA-GNIP stations in the North Pacific suggest large-scale vapor transport patterns may explain the weak relationship between air temperature and δP (Bowen and Wilkinson, 2002). With only three IAEA-GNIP sites in all of Alaska, and two in adjacent Yukon Territory (Fig. 3 inset), modern- and paleo-spatial and seasonal variability of δP is largely unknown.

2.3. Diatom oxygen isotopes as an archive of lake-water conditions

Diatoms (Class Bacillariophyceae) are composed of an amorphous silica shell ($SiO_2 \cdot nH_2O$) (i.e., "frustule") and a thin, organic layer surrounding the frustule (Round et al., 1990). The $\delta^{18}O_{diatom}$ value is dependent on the 1) temperature and 2) oxygen-isotope composition ($\delta^{18}O$) of the ambient water during diatom formation (Leng and Barker, 2006). Where the lake water $\delta^{18}O$ is known, $\delta^{18}O_{diatom}$ can be used as a palaeothermometer (Juillet-Leclerc and Labeyrie, 1987). Recent isotope analyses of paired diatom and water samples suggest that the lake water $\delta^{18}O$ - $\delta^{18}O_{diatom}$ fractionation effect is -0.2 ‰/°C (Labeyrie et al., 1984; Juillet-Leclerc and Labeyrie, 1987; Shemesh et al., 1992; Brandiss et al., 1998; Moschen et al., 2005). While these studies have constrained the general temperature dependence of fractionation between water and diatoms, quantifying temperature change from a sedimentary sequence is difficult because estimating past changes of lake water $\delta^{18}O$ requires many assumptions about regional climate, including moisture source, seasonality of

precipitation, and the E/P balance of the lake. Making assumptions about such dynamic climate conditions during the past is difficult without supporting data. Realistically, downcore changes in $\delta^{18}O_{diatom}$ reflect a combination of many climatic, and potentially non-climatic, factors. Paleoclimate interpretations from sedimentary $\delta^{18}O_{diatom}$ records should be drawn conservatively (Leng and Barker, 2006).

Diatom productivity is dependent on a host of climate and lake conditions (e.g., temperature, nutrient availability, and lake mixing regime). In temperate lakes maximum productivity, or "blooms," follows spring or autumn lake mixing when nutrients are most readily available. The seasonal timing of diatom formation is an important consideration because the isotope signature is acquired during formation. For example, in stratified lakes, surface water may become enriched in ^{18}O through the summer, and diatoms formed during early and late summer can have different isotope values (e.g., Moschen et al., 2005).

Lake water residence time and the seasonal range of δP are also important. Water in small, shallow lakes will be refreshed more rapidly than large, deep lakes. Therefore, $\delta^{18}O_{diatom}$ will be more sensitive to seasonal δP in the former and mean annual or long-term δP in the latter. However, if the seasonal range of δP of an area is low, $\delta^{18}O_{diatom}$ would be insensitive to lake residence time or the timing of diatom bloom.

3. Study site

3.1. Mica Lake

Mica Lake (informal name, 60.96° N, 148.15° W; 100 meters above sea level [m a.s.l.]) is located on Culross Island in the western Prince William Sound (PWS) of southern Alaska (Fig. 3). Whittier, AK, is approximately 29 km to the west-northwest. Mica Lake was selected because the high precipitation rate in the PWS likely limits the effect of evaporation on surface waters and the warm, maritime setting likely increases lake productivity. The lake is topographically open with numerous small stream inflows and one outflow, spilling water into a small pond ~30 m lower (Fig. 4), which discharges to the coast. The lake surface and drainage areas are 0.8 and 4.0 km^2, respectively. Lake surface water pH was 6.0 and 6.2, and secchi-disk depth was 11.2 and 13.6 m, during June 2006 and August 2007, respectively. Patchy snow cover in the watershed persisted well into July during 2006. During August 2007, snow was essentially absent from the catchment and outflow discharge was much reduced, and two of the four inflows were dry.

Mica Lake fills a glacially over-deepened basin in a granite stock surrounded by meta-sedimentary rocks (Beikman, 1980). The granite provides abundant mica, which forms a distinctive component of the sediment. The east and southern slopes descend steeply into the lake, forming cliffs at many locations. The western part of the watershed is less steep, and the northern area is all within 30 m above lake level. Slopes to the east and west sides of the watershed rise to summits 600 m a.s.l. within 0.75 and 1.25 km of the lake, respectively (Fig. 4). The steep slopes are prone to

snow avalanches and any weathered debris that accumulates on the impermeable granite substrate is likely to flush into the lake during high precipitation events, especially on the east slopes. The modern vegetation is Pacific coast forest (Ager, 1998). Sitka spruce (*Picea sitchensis*) arrived ~2.5 ka and mountain hemlock (*Tsuga mertensiana*), which is most common in the Mica Lake watershed, arrived soon after (Huesser, 1983).

3.2. Modern climate

To provide a regional climate summary, data from long-term climate stations in PWS were used to calculate monthly averages (Table 2; Fig. 5). All data were obtained from the Western Regional Climate Center of the Desert Research Institute (http://www.wrcc.dri.edu/index.html; last accessed 24 September 2007). Only sites with > 90% of data for the period 1980 – 2005 were used, which limited the number of sites to five: Seward, Whittier, Cannery Creek, Valdez, and Cordova (Fig. 3). PWS receives the highest precipitation rate during September (366 mm) and December (347 mm). The warmest (13.2 °C) and coldest (-3.2 °C) months are July and January, respectively (Fig. 5a). Using the same screening criteria, data from three interior sites, Gulkana, Snowshoe Lake, and Tonsina were used for comparison with the PWS sites. At the interior sites, precipitation is highest in July (44 mm) and August (36 mm). The warmest (13.2 °C) and coldest (-20.1 °C) months are July and January, respectively (Fig. 5b). The strong climate gradient is evidenced by reduced precipitation and increased temperature range at the interior sites.

4. Methods

4.1. Sediment core recovery, sampling, and geochronology

In June 2006, three percussion cores (7.6 cm diameter) and companion gravity cores (6.5 cm diameter) up to 3.1 and 0.3 m, respectively, were recovered from Mica Lake from depths ≤ 58 m (Table 3). Coring at site 2 (Fig. 4) was presumably halted by the bedrock as evidenced by freshly broken granite fragments lodged in the bottom of the percussion core. The percussion (MC-2) and gravity core (MC-2-C) from core site 2, here after collectively referred to as "MC-2," is the longest recovered sediment sequence and is the focus of this study. One of the three gravity cores from site 2 (core MC-2-A) was extruded and subsampled at contiguous 0.25 cm intervals in the field. All cores and bagged samples were shipped to Northern Arizona University (NAU). Cores were split, photographed, and stored at 4 °C. Sediment characteristics and tephra horizons from a fresh surface were described and assigned a Munsell soil color. For physical sediment and diatom analyses, the top 5 cm of sediment were sampled contiguously at 0.5 cm intervals, which was expanded to 5 and 10 cm spacing down to 100 and 310 cm, respectively. Samples were spaced for higher resolution upward to provide more detail, presumably, during the last two centuries (0 to 5 cm, contiguous sampling) and the last 2000 years (10 to 100 cm, 5 cm sampling) with coarse-sampling for the remainder of the core (100 to 300 cm, 10 cm sampling).

For radiocarbon analyses, 0.5-cm-thick samples were collected at 20 cm spacing, or where vegetation macrofossils were visible, sieved and dried under a

laminar-flow hood. AMS ^{14}C analyses were completed at the Keck Carbon Cycle AMS Facility, University of California, Irvine or the Lawrence Livermore National Laboratory, Riverside, CA. Contiguous 0.5 cm samples were also collected from MC-2-C for ^{210}Pb and ^{137}Cs gamma spectrometry analyses at the University of Southern California.

4.2. Lake instrumentation

Sediment traps were deployed at core site 2 at 10 and 58 m below the lake surface in June 2006 and collected and redeployed in August 2007. Water temperature loggers along side the traps and an air temperature logger on the north side of the lake (Fig. 4) recorded local water and air temperature conditions at 2 hr intervals from June 2006 to August 2007.

4.3. Regional water and top-sediment sampling

Lakes selected for water and top-sediment sampling are within 210 km of Mica Lake and range in elevation from 9 to 1160 m a.s.l. (Table 4; Fig. 3). The sampling strategy included a regional elevational gradient encompassing lakes from three climate regimes of southern Alaska: maritime, transition, and interior (Papineau, 2001). The three climate regimes are in close proximity to one another because the Chugach Mountains, rising 4000 m and spanning about 500 km, act as an effective moisture barrier, thereby causing strong temperature and precipitation gradients across zones. In general, the maritime zone receives higher precipitation (2920 mm/yr) and has lower seasonal temperature ranges (from -3.2 to 13.2 °C) when

compared to the interior zone (270 mm/yr and from -20.1 to 13.2 °C) (Papineau, 2001) (Fig. 5). Both topographically open and closed (no surface outflow), as well as glacially fed and non-glacial, lakes were sampled in nearly each climate zone (Table 4).

Water samples from lake, stream, precipitation, glacier, and snowpack were collected across south-central Alaska during the summers of 2006 and 2007 (Fig. 3). Water samples were collected in 15 mL polyethelene bottles with little or no headspace, and sealed with vinyl tape. Lake surface waters were collected from the approximate center of the lake or from the littoral zone when logistical constraints limited boat access. The bottles were kept frozen or cool whenever possible.

To investigate the modern spatial distribution of $\delta^{18}O_{diatom}$, the top 0.5 to 1.0 cm of sediment from 12 lakes was collected using a gravity corer. Logistical constraints (i.e., boat access) did not allow for top-sediment sampling at all lakes sampled for water.

4.4. Physical sediment analyses

Each sampled 0.5 cm interval from MC-2 was measured for organic-matter content (OM) by weight loss on ignition, and biogenic silica content (BSi) using a wet-alkaline extraction adapted from Mortlock and Froelich (1989). Both OM and BSi of lake sediment have been successfully used to study past changes in lake and watershed productivity (e.g., Nesje and Dahl, 2001; Hu et al, 2003; Nesje et al., 2004; McKay, 2007). The two physical sediment characteristics measure the amount of preserved biogenic material. At Mica Lake, OM and BSi provided proxies of

environmental change to corroborate $\delta^{18}O_{diatom}$ changes. BSi also helped forecast the success of the diatom isolation procedure (see below) because diatom isolation is inherently dependent on diatom abundance.

Magnetic susceptibility (MS) was measured on split-core faces at contiguous 0.5 cm intervals using a Bartington MS2 meter with Surface Scanning Sensor MS2E. MS primarily reflects the abundance of magnetic grains and was used to locate tephra horizons and confirm bulk lithology changes because tephra and minerogenic sediment contain magnetic grains, which are absent in OM and BSi.

4.5. Diatom isolation and analyses

Diatoms from 46, 0.5-cm-thick samples sampled at contiguous to 10-cm-spaced intervals were isolated and analyzed for their oxygen-isotope composition. Pure diatoms must be isolated because other lake sediments (e.g., tephra, mineral grains, organic matter) contain oxygen that would be liberated during vaporization of the sample for mass spectrometer analyses (Leng and Barker, 2006). A three-stage protocol involving chemical digestion, wet sieving, and heavy-liquid separation (Fig. 6) was adapted from Morley et al. (2004). The isolation technique was optimized to best separate diatom from the ambient sediment in core MC-2. Diatom extracts were screened for purity using a high-powered microscope, and a scanning electron microscope was used to further confirm the purity of selected intervals (Fig. 7). The 10 to 50 μm size fraction was found to be most pure because it removed clay and coarse silt.

The silica tetrahedra of diatom frustules can be divided into two parts: an outer, hydrous layer and a dense, inner layer. While oxygen in the inner layer is isotopically homogenous, the outer layer freely exchanges with the ambient water after formation (Juilliet, 1980). Therefore, the outer silica tetrahedra must be removed prior to mass spectrometry analyses to obtain an isotope value representative of lake water during formation. Numerous methods have been used to remove the outer hydrous layer, including vacuum dehydration, isotope exchange, and stepwise fluorination (see review in Leng and Barker, 2006). Most recently, a stepwise fluorination technique was designed that uses a CO_2 laser-ablation system, coupled to a mass spectrometer (Dodd et al., in press). This study is the first to employ the new method to analyze lacustrine diatoms. The new technique is rapid and requires only 1.0-2.0 mg of pure diatoms, which is less than the 5 mg typically used for stepwise fluorination techniques. $\delta^{18}O_{diatom}$ analyses were completed at the University of New Mexico, Albuquerque, NM. One in-house quartz standard, Gee Whiz ($\delta^{18}O = 12.5 \pm 0.15‰$), and an in-house diatomite standard, SR2-1B ($\delta^{18}O = 32.3 \pm 0.2‰$), were routinely run with each batch of 10-18 samples. Gee Whiz has been calibrated to the international NBS quartz standard ($\delta^{18}O = 9.6‰$). Duplicate analyses of 10 randomly selected samples from the MC-2 sequence have an average reproducibility of $\pm 0.2‰$, which is the uncertainty assigned to diatom samples analyzed over the course of this study. The results are presented as conventional permil deviations from the V-SMOW standard.

4.6. Water isotope analyses

Hydrogen and oxygen isotope ratios of water samples were measured with a Thermo-Finnigan Deltaplus XL gas isotope-ratio mass spectrometer interfaced to a Thermo-Electron Gasbench II headspace equilibration device at the Colorado Plateau Stable Isotope Laboratory (http://www.isotope.nau). Analytical precision on internal working standards was ± 1‰ for δD and ± 0.1‰ for $\delta^{18}O$. Hydrogen and oxygen isotope ratios are presented in permil deviations from the V-SMOW standard.

5. Modern meteorological and water and diatom isotope analyses

5.1. Mica Lake meteorological correlations

The air temperature logger at the north end of Mica Lake operated continuously from 3 July 2006 to 12 August 2007. These data show that the warmest (15.0 °C) and coldest (-11.8 °C) days occurred on 8 August 2007 and 7 January 2007, respectively. The average annual temperature (3 July 2006 to 2 July 2007) was 2.8 °C. Daily temperature data from Whittier (Fig. 3) is strongly correlated (r = 0.97) with temperature at Mica Lake (Fig. 8a). The seasonal relationships are strong as well; during the summer, the relationship between Mica Lake and Whittier temperature is non-linear with higher-amplitude temperature fluctuations at Whittier than at Mica Lake. From the daily average temperate data, lapse rates (lapse rate between two sites = Δ temperature ÷ Δ elevation) were calculated, and the daily temperature at the median elevation of the Mica Lake watershed (364 m a.s.l.) was calculated. Median watershed elevation is defined as the elevation halfway between the lake elevation

and the highest elevation within a watershed. These temperatures were then combined with precipitation data from Whittier to estimate the number of days with snowfall at the Mica Lake watershed (gray vertical bars, Fig. 8b). I assumed that, when precipitation was recorded at Whittier, it extended to Mica Lake, which is probably correct considering their proximity (29 km). These analyses show that days with snowfall make up 70% of precipitation days at Mica Lake, and that snowfall occurs between mid-September and early June, with peak precipitation during mid-September to early November, early December to February, and early April to mid-June.

5.2. Regional water isotope data

δW values in water collected from south Alaska during the 2006 and 2007 summers range from -22.6 to -5.9‰, and -176.1 to -37.6‰ for $\delta^{18}O$ and δD, respectively (Fig. 9a). Data from each of the three climate zones define local water lines (Fig. 9b-c; Fig. 10b). Broadly, δW values trend from heavy to light and back to heavy values along the south-to-north moisture pathway (Fig. 10a). In PWS, $\delta^{18}O$ and δD define the local meteoric water line (LMWL), which is parallel to the global meteoric water line (GMWL) (Fig. 9b). In the transitional climate zone, $\delta^{18}O$ and δD are generally lower and the data define a local evaporation line (LEL), which has a slope (~6) less than the LMWL and GMWL (8) (Fig. 9c). The lower δW values reflect the cooler temperatures at the higher sites sampled in this climatic zone and rain-out as moisture is transported north over the Chugach Mountains (Fig. 10a). The reduced slope is due to enrichment of surface water in $\delta^{18}O$, relative to δD caused by

evaporation (Gat, 1981) and therefore departs from the GMWL. Similarly, water from the interior sites is relatively heavy, with a slope (~6) parallel to the LEL (Fig. 9d). Heavy $\delta^{18}O$ and relatively light δD values at interior sites are due to evaporation.

In surface waters, deuterium excess (d.e. = $\delta D - 8\delta^{18}O$) decreases because evaporation affects fractionation of hydrogen and oxygen differently (Dansgaard, 1964). For example, in the Canadian arctic and Baffin Island, evaporation during the summer decreases surface water deuterium excess by as much as 15‰ (Gibson et al., 1993; Sauer et al., 2001). The trend of decreasing deuterium excess from south to north supports the idea that greater evaporation occurs farther inland (Fig. 10a). The large difference in precipitation rates between PWS and interior sites and warmer summers at interior sites (Fig. 5) are likely causes of the regional trends.

5.3. Prince William Sound lake and watershed characteristics and δW data

δW values of PWS lakes range from -134 to -93‰, and -17.5 to -12.9‰ for δD and $\delta^{18}O$, respectively, a relatively wide range for closely located sites that experience relatively similar temperatures and precipitation rates. To better explain these data, PWS δW values were compared with lake and watershed characteristics (Fig. 11; Table 5). Lake and watershed area, lake elevation, median watershed elevation, and the presence or absence of glaciers were tabulated from maps and aerial photos. The lakes were divided into glacial and non-glacial groups because lake water in glaciated catchments inherits meltwater derived from past precipitation during summer melting. Most lake characteristics are covariant with one another, with

stronger covariance for glacial than non-glacial lakes (Table 5). The correlation between δW and lake and watershed elevations are weaker for glacial than non-glacial lakes, but the correlation between lake and watershed area is stronger for glacial lakes.

The strongest correlations are between δW and elevation. Median watershed is more strongly correlated than lake elevation (Table 5; Fig. 11). For non-glacial lakes, the r-values for δW and median watershed elevation are -0.95 and -0.90 for $\delta^{18}O$ and δD, respectively, and are highly significant ($p < 0.0001$ for $\delta^{18}O$; $p < 0.01$ for δD). For glacial lakes, the correlations between δW and median watershed and lake elevation are not as strong, and are not significant at the 90% confidence level (Table 5). The stronger correlation with median watershed elevation than for lake elevation is further evidence that PWS δW integrates and reflects δP.

The slope of the regression line for median lake elevation vs. lake water $\delta^{18}O$ is -0.76‰/100 m for non-glacial lakes. This gradient is similar to the values reported from snow samples collected between 1750 and 3350 m a.s.l. in the St. Elias Mountains (-0.7 to -0.6‰/100 m) (Holdsworth et al., 1991). Vertical isotope models and measurements from the coast to ~1000 m a.s.l. suggest a slope of -0.95‰/100 m (Fig. 9a in Fisher et al., 2004).

At Mica Lake, surface, bottom, inflow, and outflow water (n = 15) have a narrow range of $\delta^{18}O$ values (Fig. 10c). This observation, combined with similarity to the GMWL, suggests that the lake is well mixed and evaporation does not greatly alter its isotopic values.

5.4. Diatom oxygen isotopes from modern lake sediment

Pure diatoms were isolated from core tops of four lakes and trap sediment from one lake in the study area (Table 6). Four of the lakes are located in the PWS and are topographically open; one lake is located ~150 km north of PWS in the interior and is topographically closed. The diatom abundance was too low in the top sediment from most surveyed lakes to be used for $\delta^{18}O$ analysis. The $\delta^{18}O_{diatom}$ values from top and trap sediment range from 22.7 to 29.8‰ (Fig. 12; Table 6). Compared with the water from the same lake, the diatoms have an oxygen-isotope fractionation (Δ = $\delta^{18}O_{diatom}$ - lake water $\delta^{18}O$) between 38.5 and 42.8‰.

Modern lake conditions were compared with $\delta^{18}O_{diatom}$. Mean annual and summer (JJA) air temperatures were projected for each lake using a standard lapse rate and temperatures from the nearest climate station with complete data for the last 15 yr (Table 6). A moist (6°C/km) and dry (10°C/km) adiabatic lapse rate was used for the PWS and interior sites, respectively. The 15 yr climate window was selected to coincide with the estimated age of the top 0.5 - 1.0 cm core-top sediment samples. The summer temperature during the ice-free season (JJA) was selected because it likely coincides with the timing of diatom productivity. The interior site was excluded from correlations because it is a closed lake within a different climate regime (low precipitation and large temperature range) than PWS sites (high precipitation and limited temperature range) (Fig. 5). Under these conditions, the P/E balance at the lake will likely influence the δW. This limited data must be interpreted with caution, but provide a baseline on which to build.

On the basis of just four samples, $\delta^{18}O_{diatom}$ correlates most strongly with lake water $\delta^{18}O$ ($r = 0.99$, $p < 0.01$), median watershed elevation ($r = -0.97$, $p < 0.1$), mean air temperature ($r = 0.94$, $p < 0.1$), and summer air temperature ($r = 0.87$, $p = 0.13$) (Fig. 12a - 12d) and are discussed below. The strong empirical relationship between $\delta^{18}O_{diatom}$ and lake water $\delta^{18}O$ (Fig. 12a) suggests that lake water $\delta^{18}O$ is the dominant control on $\delta^{18}O_{diatom}$ from these sites. Comparison of top sediment diatoms, representing ~15 yr of sedimentation, and lake water, representing < 10 yr of summer lake water, may be inaccurate because the mean age of diatoms is probably older than lake water.

The relationship between $\delta^{18}O_{diatom}$ and median watershed elevation is stronger when compared to lake elevation (Fig. 11e and 11f) and has a slope of -1.73‰/100 m, which is nearly 2.5 times greater than that observed between lake water $\delta^{18}O$ and median watershed elevation (-0.76‰/100 m) (Fig. 11b). While keeping in mind that the steep slope of $\delta^{18}O_{diatom}$ versus median watershed elevation is calculated from only four samples, the increase in slope suggests an amplification of $\delta^{18}O_{diatom}$ enrichment (depletion) at lower (higher) elevation during the last ~15 yr. Analyses between lake and watershed characteristics and $\delta^{18}O_{diatom}$ provide no interbasin mechanism to explain the greater increased slope (Table 5). If low and high elevation sites receive moisture with different transport histories (e.g., distance traveled and moisture source), the gradient could be explained by non-temperature controls. For example, if high elevations receive on average more long-traveled moisture (e.g., Bering Sea), greater rain-out would cause more depleted $\delta^{18}O$ of lake water values relative to low elevation sites that receive only local moisture (e.g.,

Gulf of Alaska). Therefore, the increased slope of lake water $\delta^{18}O$ vs. $\delta^{18}O_{diatom}$ could be explained if lake water $\delta^{18}O$ from my summer collections reflect a time when different elevations received moisture from the same source and pathway, whereas, $\delta^{18}O_{diatom}$ values reflect the integration of mixed moisture and pathway histories. This hypothesis seems most logical because storm tracks are known to vary in the region due to shifts in the position of the AL (Table 1; Fig. 1) and because lakes incorporate multiple years of precipitation so lake water $\delta^{18}O$ likely reflects 'average' moisture from different storm tracks.

The slopes of mean annual and summer air temperature vs. $\delta^{18}O_{diatom}$ (Fig. 12b and 12c) are also steeper than would be predicted by simply combining the known relationship between lake water $\delta^{18}O$ and $\delta^{18}O_{diatom}$ (-0.5 to -0.2 ‰/°C_{water}) (e.g., Moshen et al., 2005) with the global range of temperature-dependent fractionation of δP (0.2 to 0.9‰/°C) (e.g., Rozanski et al., 1993). Applying this range, the highest value (0.7‰/°C) falls well short of the observed relationship between lake water $\delta^{18}O$ and $\delta^{18}O_{diatom}$. Again, this observation suggests additional feedbacks between lake water $\delta^{18}O$ and $\delta^{18}O_{diatom}$ that are not presently understood, but are not likely due to decreased temperature with increased elevation.

Uncertainties inherit to these analyses include: 1) the sparse dataset (n = 4), 2) the limited temperature range of the sample sites, 3) the site temperature extrapolation, 4) the age of the modern diatom samples, which may encompass more or less than the 15 yr estimate, 5) the differential timing of diatom bloom at each lake, and 6) the presently unknown diagenetic effects. Lacking data to better understand between-site variations in $\delta^{18}O_{diatom}$, neither the relationships between

$\delta^{18}O_{diatom}$ and lake water $\delta^{18}O$ nor median watershed elevation can be used for quantitative interpretations of climate from downcore variability of $\delta^{18}O_{diatom}$.

6. Lake core results and interpretation

6.1. Core chronology

6.1.1. ^{210}Pb and ^{137}Cs profiles

Two gravity cores (MC-2-A and -C) were taken from the same site and measured for ^{210}Pb and ^{137}Cs activities (Table 7; Fig. 13). MC-2-A was extruded and sub-sampled in the field at contiguous 0.25 cm intervals; MC-2-C was transported to NAU where it was split and sampled at contiguous 0.50 cm intervals. The two cores show similar, first-order trends, with ^{210}Pb and ^{137}Cs decreasing with depth, which supports the general reproducibility of the analyses. In detail, however, the differences in the two ^{210}Pb profiles suggest a range of sedimentation rates. In core MC-2-A, the relatively constant downcore ^{210}Pb activity below 1.5 cm suggests a high sedimentation rate. Conversely, the decrease of ^{210}Pb from 2.75 to 3.25 cm in core MC-2-C suggests a rapid decrease in sedimentation rate (Fig. 13a). The lithology of this section of the core is uniform and there is no evidence of sedimentation rate changes. Using a constant rate of supply (CRS) model for core MC-2-C suggests an average sedimentation rate of 0.41 mm/yr, but a CRS model could not be constructed for MC-2-A because the total excess ^{210}Pb was not measured. The geochronological significance of the ^{210}Pb profile is presently unclear.

The ^{137}Cs profiles are also difficult to interpret. In general, ^{137}Cs should rise from background values, reach a maximum, and then decrease to lower values near the core top. The rise, crest, and descending trends correspond to the onset and peak of nuclear weapons testing in the 1950's and 60's. The 1986 Chernobyl event has been recognized in Northern Hemisphere glacier ice and lake sediments as a second, younger peak in ^{137}Cs profiles (e.g., Pinglot and Pourchet, 1995; Schiff et al., 2008). The high values in the top 0.5 cm of MC-2-A suggest that the 1963 peak is captured within this interval, whereas the initial rise at 2.75 cm and peak at 1.75 cm in MC-2-C occurs deeper in the core (Fig. 13b). Therefore, the implied sedimentation rate from MC-2-A is an order of magnitude less than from MC-2-C. Taken together the ^{210}Pb and ^{137}Cs data suggest sedimentation rates between 0.16 and 0.75 mm/yr, which brackets the rate estimated by ^{14}C ages (0.30 mm/yr; see below). However, with no stratigraphic evidence to support the sedimentation rate changes implied by the ^{210}Pb profiles, and considering the contrasting ^{137}Cs profiles, no accurate geochronological information can be obtained from these data.

6.1.2. ^{14}C age model

Sixteen ^{14}C ages were calibrated to calendar years using the IntCal04 calibration curve (Reimer et al., 2004) and CALIB (v 5.0.2; Stuiver and Reimer, 1993). I used the median probability age output by CALIB as the single best estimate of the central tendency of the calibrated age (Telford et al., 2004), and report all ages in reference to cal yr AD 1950 (yr BP). Thirteen calibrated ages on terrestrial and aquatic macrofossils (Table 8) and the age of the sediment surface (0 cm = -56 yr BP) were

combined to construct a depth-age model for core MC-2 (Fig. 14). Three ages were not included in the age model because the terrestrial vegetation yielded ages older than underlying ages, or they were from a sand-rich layer, interpreted to be an avalanche deposit (see below). A spline fit was constructed using formulations from Heegaard et al. (2005) and the statistical software R (http://cran.r-project.org; last accessed 20 December 2007). The Heegaard procedure performs well for lake sediment that contains abundant tephra layers (Schiff et al., 2008). The model takes into account both the uncertainty in the calibrated ages as well as the uncertainty of how well the age represents a particular core level. In addition to an age-depth model, the procedure generates the 95% confidence intervals. The model requires the selection of a k-value, which dictates how closely the spline approaches each calibrated age. A high k-value will closely follow the ages, and the spline will have more flexure whereas low k-values produce a rigid spline. A k-value of 7 was selected for the MC-2 core because it is the lowest value that contains most of the 2 σ ranges of the calibrated ages, and has relatively low model residuals, which is the difference between the calibrated and estimated age of each dated levels. Using this age model, the base of the core is extrapolated to 9910 yr BP and the average sedimentation rate is 0.30 mm/yr. Therefore, each 0.5 cm sample represents ~15 yr of sedimentation. The average age uncertainty based on the 95% confidence interval is ± 112 yr. The basal age provides a minimum age of deglaciation at Mica Lake.

6.2. Core description

Based on MS, OM, BSi, and physical descriptions, sediment from MC-2 was divided into three units: tephra, massive gyttja, and sand-rich layers (Fig. 15). Massive gyttja units are brown (10YR, 2/2 or 3/4) with some color banding (10YR 4/2), whereas sand-rich units include sand, pebbles, and abundant terrestrial vegetation macrofossils and exhibit a wide spectrum of colors. Upper and lower contacts between all units are sharp, although the uppermost sand-rich layer grades into the overlying massive gyttja (Fig. 15). The MC-2 sequence contains 91% gyttja, 5% sand-rich layers, and 4% tephra (Fig. 16). The gyttja contains relatively high OM (19%) and BSi (5%), with low average MS (15 ± 19 SI, n = 565). Following the sampling strategy outlined above, only one sand-rich layer was sampled for OM and BSi and has lower OM (15%) and BSi (1.7%). Sand-rich layers have higher average and more variable MS (120 ± 143 SI, n = 34). Tephra horizons exhibit the highest average MS values (190 ± 155 SI, n = 23), and were not analyzed for OM and BSi. OM and BSi range from 5 to 35% and 1.7 to 7%, respectively, and the two are positively correlated (r = 0.52) (Fig. 16 graph inset). OM and BSi data are provided in Appendix B-1. Sand-rich layers occur at three depths: 20.5 - 27.5, 185.5 - 196.0, and 280.0 - 280.5 cm (tube depth) (Fig. 16). Coarse flecks of mica are visible on the surface of gyttja and sand-rich layers.

The abundant macrofossils of terrestrial vegetation and coarse grains in sand-rich layers suggest that these deposits are avalanche derived. Steep, sparsely vegetated slopes (Fig. 4), with abundant snowfall and an ice-covered lake could facilitate transport of such coarse material to core site 2. The presence of

minerogenic particles > 1 mm and macroscopic plant remains have been used as proxies for snow avalanches. Lake sediment studies in Norway document snow-avalanche deposits in lake basins with steep slopes (e.g., Seierstad et al., 2002; Nesje et al., 2007). These studies corroborate the link between coarse-particle sedimentation and terrestrial macrofossils with avalanche deposits.

Six visible tephra layers, ranging from 0.5 to 2.5 cm thick, are marked by high MS values (Table 9; Fig. 16). All have sharp upper and lower contacts. The uppermost tephra was used to splice together the percussion and gravity cores and suggests that 6.5 cm was lost during percussion coring. The tephra and sand-rich layers, interpreted as instantaneous deposits, were removed from the sediment thickness to determine an adjusted depth below lake floor (blf) for core MC-2 (Fig. 16).

A hemlock needle directly below a tephra layer (2) at 35.25 cm (tube depth) has a calibrated age of 1125 yr BP (Table 9; Fig. 14 inset). The tephra was initially thought to correlate with the White River Ash (WRA), which has been dated to 1147 yr BP from ^{14}C ages on trees buried by tephra in growth position near the summit vent of Mt. Churchill volcano (Clague et al., 1995). However, preliminary geochemical analyses suggest the tephras are not correlative (K. Wallace, personal communication). The similar age of tephra 2 from Mica Lake and the WRA is an important discovery because tephra deposits found around this time period are often correlated to the WRA with little geochemical evidence.

From the k = 7 age model, a 0.5-cm-thick tephra layer (3) at 144.75 cm (tube depth) has an interpolated age of 3950 yr BP, which is near the age of Hayes tephra

deposits found in south Alaska (e.g., Schiff et al., 2008). Visual inspection of the sample shows characteristics (e.g., mineral assemblage) with known Hayes deposits (K. Wallace, personal communication). However, without geochemical data, identifying the deposit as Hayes tephra remains preliminary.

6.3. OM and BSi interpretation

Low sedimentation rates and inconclusive ^{210}Pb and ^{137}Cs ages from the upper part of the Mica Lake cores prevent a detailed comparison between the proxy data and meteorological data. Therefore, changes in OM and BSi provide only a qualitative interpretation of environmental conditions at Mica Lake. Assuming that OM and BSi are a proxy for productivity at Mica Lake, then productivity increased gradually between 9.6 and 2.5 ka then decreased to 0.1 ka, although neither the long-term increase nor decrease are monotonic (Fig. 16). The coefficient of variability is greater for OM (32%) than for BSi (20%). The greater variability in OM suggests it is sensitive or controlled by different environmental factors than BSi. Diatom abundance is influenced by lake productivity related to water temperature, length of ice-free season, rainfall, and nutrient availability (Anderson, 2000). The greater variability may suggest that OM is influenced by the amount of terrestrial vegetation transported to the lake from the adjacent, steep-walled watershed. Increased terrestrial components of vegetation transported to the lake via episodic slope failure and avalanches would likely cause greater variations in OM than BSi if diatom abundance is more dependent on intralake factors. The preservation of at least three avalanche deposits in MC-2 is evidence that lake sedimentation is influenced by such

watershed slope processes. Without further evidence (e.g., C:N ratios) this explanation is only speculative.

6.4. Diatom oxygen isotopes from Mica Lake

Forty-six downcore $\delta^{18}O_{diatom}$ values from MC-2 range between 25.2 and 29.8‰ (Fig. 17a). Prior to 2.5 ka, the values range by only 2.2‰. At 2.5 ka, $\delta^{18}O_{diatom}$ exhibits a strong shift to values that vary as much as 4.6‰. The youngest sample, which represents the last ~15 yr contains the highest $\delta^{18}O_{diatom}$ value at 29.8‰. Within the analytical precision of the laser-extraction technique (±0.2‰), only one other sample, at 6.4 ka, is comparable (Fig. 17a).

7. Controls on diatom oxygen-isotope variability at Mica Lake

The large (4.6‰) variation in $\delta^{18}O_{diatom}$ from MC-2 cannot be due wholly to changes in lake water temperature. Applying the lake water $\delta^{18}O$ - $\delta^{18}O_{diatom}$ fractionation of -0.2 ‰/°C and assuming no change in δW suggests a lake-water-temperature range of ~23°C during the Holocene, which is untenable. Therefore, alternative controls must be considered to explain the $\delta^{18}O_{diatom}$ variability.

7.1. Non-climatic controls

Diagenetic effects have been reported in studies that compare trap- and sedimentary-diatom oxygen isotopes (Schmidt et al., 1997, 2001; Moschen et al., 2006). These studies found a slow-acting maturation of diatoms that led to enrichment of $^{18}O_{diatom}$

after deposition. The authors attribute the enrichment to silica dissolution and dehydroxylation, and suggest that $\delta^{18}O_{diatom}$ records with long-term trends of enrichment with age should consider diagenetic effects as a leading explanation. No studies investigating diagenetic effects have reported lower $\delta^{18}O_{diatom}$ values in older sediment, however. Furthermore, backscattered electron images show no obvious dissolution of modern (Fig. 7a; 0 cm) or mid-Holocene (Fig. 7b; 75 cm) diatom frustules from MC-2. This observation, combined with the lack of a long-term trend in the MC-2 record suggests that diagenetic effects are absent or undetectable at Mica Lake.

Diatom habitat and taxonomic (vital) effects may influence $\delta^{18}O_{diatom}$. Because diatoms live in both benthic and planktonic settings, they experience different temperatures throughout the year (Round et al., 1990). Benthic and planktonic diatoms formed at the same time could have different isotope signatures, particularly if the lake water $\delta^{18}O$ differs between habitats. At Mica Lake, however, surface and bottom water during the June 2006 and August 2007 had nearly identical $\delta^{18}O$ values (Fig. 10c), suggesting the lake is well mixed during the late spring and summer.

Vital effects have yet to be documented for $\delta^{18}O_{diatom}$ and are expected to be less than the analytical error of fluorination techniques (Leng and Barker, 2006). In one of the most detailed $\delta^{18}O_{diatom}$ investigations to date, Moschen et al. (2005) analyzed diatoms of three separate size ranges, each inferred to comprise different diatom taxa. They found the same lake water $\delta^{18}O$ - $\delta^{18}O_{diatom}$ fractionation for each size fraction, suggesting that diatoms are not influenced by a vital effect. From Mica

Lake, only the 10-50 μm size fraction was analyzed. While this size fraction was selected primarily because of its purity, this narrow size range also likely limits the number of taxa analyzed (Battarbee et al., 2001). In sum, a $\delta^{18}O_{diatom}$ vital effect is likely nonexistent or undetectable in Mica Lake. An investigation of diatom flora from MC-2 is in progress and will provide information to better address the potential influence from habitat and vital effects by assessing the relative proportion of benthic and planktonic taxon changes downcore.

7.2. Climatic controls

The inability of water temperature – diatom fractionation and non-climatic factors to fully explain the large variability of Holocene $\delta^{18}O_{diatom}$ values suggests that the δW at Mica Lake has varied over the last 9600 yr, and largely determined the sedimentary $\delta^{18}O_{diatom}$. This is further supported by two additional observations from this study: 1) there is no apparent correlation between lake productivity (i.e., OM and BSi) and $\delta^{18}O_{diatom}$ at Mica Lake (Fig. 16, inset graphs), even though productivity is at least partly determined by temperature; and 2) the relationship between lake water $\delta^{18}O$ and $\delta^{18}O_{diatom}$ is strong (Fig. 12a) whereas the temperature relationships are inexplicable (Fig. 12b and 12c). The PWS slope of lake water $\delta^{18}O$ versus $\delta^{18}O_{diatom}$ also encompasses the entire range of Holocene $\delta^{18}O_{diatom}$ values from MC-2. The two primary controls on lake water $\delta^{18}O$ are the P/E balance and the $\delta^{18}O$ inflow to the lake, both of which vary with climate.

7.2.1. P/E balance

The P/E balance and therefore lake hydrology strongly controls δW of lakes (Gat, 1981). δW data from the surveyed lakes exemplify this effect: interior lakes, receiving low precipitation are topographically closed (Table 4), and evaporation at these sites favors δD over $\delta^{18}O$, which shift values from the GMWL (Fig. 9d) (Gat, 1981). In contrast, lakes in the PWS may receive an excess of 5 m of precipitation a year (Fig. 5), and all but one of the surveyed lakes is topographically open (Jerome Lake; Table 4). A small, topographically closed pond 200 m north of Mica Lake ("MP" Fig. 4) was sampled in August 2007 and demonstrates the effect of summer evaporation on surface water; the $\delta^{18}O$ is 4.3‰ higher than nearby Mica Lake (Fig. 10c). Surface and bottom water collected in June 2006 and August 2007 do suggest a small progressive isotopic enrichment of surface water from summer evaporation. δW values of bottom water are nearly identical between summers (-13.2 and -13.4‰), whereas the surface water from August 2007 is 0.5‰ enriched relative to June 2006. The enrichment is small when compared with the late Holocene 4.6‰ range of $\delta^{18}O_{diatom}$ at Mica Lake, and is irrelevant if diatom blooms always occur during the late spring, prior to progressive evaporation through the summer months. Furthermore, surface water inflow into Mica Lake collected during the summer is indistinguishable from Mica Lake surface water (Fig. 10c).

Using a range of precipitation rates from 3 to 7 m/yr, which encompasses the observed rate at Whittier during the last 25 yr (average = 5.5 m/yr), and assuming that evapotranspiration is less than 0.5 m/yr, which is typical for south Alaska

(Newman and Branton, 1972), the lake water residence time is less than 5 yr at Mica Lake. Lakes with such low residence time are relatively unaffected by evaporation.

Taken together, the high precipitation receipt, short water residence time, nearly homogenous δW at Mica Lake (Fig. 10c), and overlap with the local meteoric water line (Fig. 9), suggests that the modern δW is not strongly affected by evaporation and instead is controlled largely by δP. This conclusion is further supported by the long-term $\delta^{18}O_{diatom}$ record from Mica Lake. When strongly influenced by evaporative effects, δW is typically variable and elevated, whereas the opposite is true of wet periods (Leng and Marshall, 2004). At first glance, therefore, the increased late Holocene variability in $\delta^{18}O_{diatom}$ at Mica Lake (2.5 ka to modern; Fig. 17a) could reflect increased evaporation. On the other hand, the shift to lower $\delta^{18}O_{diatom}$ values following 2.5 ka and the coincidence with the increased variability is inconsistent with the hypothesis of increased evaporation.

7.2.2. Changes in δP at Mica Lake

Outside of the tropics, where the 'amount effect' is dominant, δP is determined by local air temperature, but can also be influenced by changes in seasonality of precipitation and changes in moisture source (Araguás-Araguás et al., 2000). Realistically, each factor affects δP to some degree, and are discussed individually to determine which controls are most influential.

7.2.2.1. Seasonality of precipitation

As previously discussed, ~70% of precipitation received at the Mica Lake watershed is snow that falls between mid-September and early June (Fig. 8). Therefore, δP (and δW) at Mica Lake is likely weighted towards winter precipitation. Seasonal differences in δP could affect δW if the seasonality of precipitation has varied. The relatively sparse IAEA-GNIP data available for the North Pacific region (Fig. 3 inset) provide some insight into the seasonal range of δP in south Alaska. The maritime climate at the Adak IAEA-GNIP station, located 2000 km to the west is most similar to Mica Lake. Between 1945 and 1970, the warmest (10.8 °C) and coldest (0.6 °C) months at Adak were July and February, respectively, whereas the wettest (199 mm) and driest (78 mm) months were December and July, respectively (Vose et al., 1992). These data are similar to the PWS, where the minimum and maximum seasonal temperatures are within 3 °C of Adak temperatures and maximum precipitation rates occur in late fall and minimum precipitation rates occur in early summer (Fig. 5a). Other sites (Bethel, Barrow, Mayo, and Whitehorse) are located in different climate regimes (Papineau, 2001) (Fig. 3 inset).

The Aleutian Islands are strongly influenced by the AL (Rodionov et al., 2005), although its expression at Adak is inverse to the AL expression in PWS (Fig. 1b). Correlations between the NPI and Adak DJF air temperature ($r = 0.49$) and precipitation ($r = 0.52$) are reverse to Whittier DJF air temperature ($r = -0.67$) and precipitation ($r = -0.49$). All correlations are significant at the 99% confidence level. IAEA-GNIP data collected between 1962 and 1973 record mean summer (JJA) temperature at Adak that is 9 °C higher than winter (DJF) temperatures, whereas

mean $\delta^{18}O$ is 0.4‰ higher in summer compared to winter. The correlation between monthly temperature and $\delta^{18}O$ in precipitation is weak ($r = 0.26$) and is not significant at the 90% confidence level. The relatively small seasonal range in $\delta^{18}O$, despite the large temperature range and the weak correlation between the two, suggests that factors other than temperature strongly influence δP at Adak. Applying the ^{18}O - air temperature fractionation from the IAEA-GNIP global dataset (0.65‰/°C; Rozanski et al., 1993) to the 9°C seasonal temperature range implies a range of 5.9‰ between summer and winter, which is an order of magnitude greater than what is recorded. The 'amount effect,' on the other hand, is more strongly correlated in the Adak dataset: monthly $\delta^{18}O$ is inversely related to the amount of precipitation ($r = -0.50$, $p < 0.1$). If the Adak data are representative of conditions at Mica Lake, higher $\delta^{18}O_{diatom}$ might represent decreased precipitation, but is likely insensitive to changes in seasonality of precipitation. The climatic similarity between Adak and PWS is not a substitute for δP from PWS. To further investigate the amount effect in the North Pacific, a phenomena that is common at low latitudes, year-long collections are needed.

7.2.2.2. Air temperature

The global relationship between δP and temperature (i.e., 'Dansgaard effect') ranges between ~0.2 and 0.9‰/°C (Rozanski et al., 1993). Applying this slope to the range in $\delta^{18}O_{diatom}$ at Mica Lake (~4.6‰) suggests a shift of 5 to 23 °C during the late Holocene. The upper estimate is not plausible, whereas the lower estimate is similar to the DJF temperature range observed between the ten strongest and weakest AL

years at climate stations in south Alaska (Fig. 1b). The paucity of IAEA-GNIP data from the region prevents an accurate measure of the influence that air temperature has on δP. These results point to the need for a more extensive collection of waters from south Alaska, especially in the winter.

7.2.2.3. Change in moisture source

The increase in the range of $\delta^{18}O_{diatom}$ values between the mid-19th century to present (4.6‰) from MC-2 may more reasonably be explained by changes in moisture source. Specifically, moisture from the west and north Pacific delivered by zonal (west-to-east) flow is longer-traveled and likely more depleted than moisture delivered by meridional (south-to-north) flow, which for south Alaska is likely from the Gulf of Alaska (Cayan and Peterson, 1989). Moisture from zonal flow crosses southwest Alaska and is susceptible to rain-out as it passes over the land, whereas moisture from meridional flow travels over the Gulf of Alaska and rain-out is significantly less. Furthermore, the Bering Sea probably contributes more moisture under zonal than meridional flow and is likely more depleted isotopically because of generally colder Bering Sea winter temperatures compared to Gulf of Alaska temperatures (Locarnini et al., 2006). All available IAEA-GNIP data from Bethel (1962-1965) show that, during the winter (DJF) $\delta^{18}O$ of precipitation is about 6‰ lighter than at Adak, and that Bethel DJF air temperatures are about 14 °C cooler than at Adak. The cooler temperature and lighter isotope values suggest that Bethel is more influenced by the Bering Sea while Adak is more influenced by the Pacific. Without more complete collections of precipitation from storm tracks originating

from the two moisture sources, I cannot provide a quantitative estimate of the change in δP. Nevertheless, δP changes from shifting moisture source are generally greater than from temperature changes over the same time period (e.g., Terranes and McKenzie, 2001).

7.3. Links to the AL

I suggest that variability in $\delta^{18}O_{diatom}$ at Mica Lake is largely controlled by the location of the moisture source during the winter, which is closely linked to the strength and position of the AL. The location of storm tracks during the winter months are known to vary between strong and weak AL years (Rodionov et al., 2005). During strong AL years, most storms tracks that intersect south Alaska have a south-to-north trajectory and the moisture contribution from the Gulf of Alaska is likely large (Fig. 1a). Precipitation during strong AL years is likely enriched in ^{18}O because the moisture is short-traveled. During weak AL years, storm tracks are more often divided into two loci and the south-to-north storm trajectory is less prominent (Fig. 1a). The weaker meridional flow might allow zonal flow to deliver moisture from a more western or southwestern, North Pacific source (e.g., Bering Sea) to reach south Alaska. Because this moisture would have been: 1) farther traveled, 2) crossed an extensive landmass (~ 700 km), and 3) sourced from cooler waters, it would be relatively depleted in ^{18}O. Furthermore, air temperature in south Alaska during strong AL years is about 5 °C warmer than weak AL years (Fig. 1b), which supports the hypothesis of greater meridional flow. As previously mentioned, the increased temperature would likely cause increased $\delta^{18}O$ and the seasonal variability

of $\delta^{18}O$ at the coastal IAEA-GNIP site is low (0.4‰), so greater winter precipitation during strong AL years would not greatly reduce the annual $\delta^{18}O$ average.

Using this interpretation, the Mica Lake $\delta^{18}O_{diatom}$ record suggests that the moisture delivery to south Alaska has shifted between zonal and meridional flow during the last 2.5 ka (Fig. 17a). Low $\delta^{18}O_{diatom}$ values reflect zonal flow. Before 2.5 ka, the record is relatively stable and has generally heavy $\delta^{18}O_{diatom}$ values, suggesting mainly meridional flow. Meridional flow is likely associated with a strong and eastward AL, which is supported by the tendency of storms to track south-to-north during strong AL years (Rodionov et al., 2005).

8. Comparisons with other North Pacific climate and paleo-isotope records

8.1. Late Holocene climate variability

Paleoclimate records across the North Pacific from lake sediments (e.g., Hu et al., 2001; Spooner et al., 2002; Cockburn and Lamoureux, 2007; McKay, 2007), glacier advances (e.g., Wiles et al., 2001), and tree rings (e.g., Wilson et al., 2007) suggest late Holocene climate variability. Most records point to some influence from the variability of the AL, usually building on the relationship between changes during the 20th century and proxy data (e.g., Anderson et al., 2005; McKay, 2007). For example, in a summary of pollen records from northwest North America, Spooner et al. (2003) showed that the occurrence of far-traveled pollen increased at multiple sites across northwest British Columbia between ~3 ka to present; the likely mechanism is thought to be a long-lasting phase of strong AL because warm air is

more frequently carried inland during strong AL years and positive correlations between the AL and instrumental temperature records were found. Climate records also link ENSO variability and other indicators of equatorial convective activity to the strength of the AL (White and Walker, 1973; Giese and Carton, 1999; Moore et al., 2003), and an increase of ENSO frequency throughout the Holocene suggests a trend towards increased instability of the inter-tropical convergence zone (Moy et al., 2002; Koutavas et al., 2006), influencing wintertime conditions in the North Pacific (Desar et al., 2004). Accumulation rates at Mt. Logan between 1948 and 1987 are correlated with warm-phases of ENSO, which correspond to increased south-to-north storm trajectories in the North Pacific (Moore et al., 2003). Similar to these Pacific paleoclimate records, the large variability of $\delta^{18}O_{diatom}$ at Mica Lake suggests dynamic pattern of atmospheric circulation during the late Holocene.

8.2. Paleorecords of δP

Paleorecords of δP from the North Pacific region are few, but a connection to large-scale atmospheric circulation is beginning to emerge. Oxygen isotope ratios of authigenic carbonate ($\delta^{18}O_{ca}$) from Holocene sediment of Jellybean Lake, Yukon Territory, Canada (Fig. 3 inset) range by ~2‰ (Fig. 17b), which is too large to be explained by changing water temperatures (Anderson et al., 2005). Rather, $\delta^{18}O_{ca}$ at Jellybean is interpreted as a proxy for the intensity and position of the AL. During times of weak AL, less rain-out occurs because zonal flow carries moisture parallel to the coastal mountains to reach Jellybean Lake. During times of strong AL, meridional flow brings moisture directly against and over the St. Elias Mountains,

causing greater distillation. Therefore, strong AL years are recorded as low $\delta^{18}O_{ca}$ values. At Marcella Lake, an evaporative-sensitive lake in Yukon Territory, Canada (Fig. 3 inset), oxygen isotopes of endogenic carbonate record effective moisture (Anderson et al., 2007). The data suggests drier conditions occur during times of strong AL because meridional flow brings stronger leeward winds to the Yukon Territory. Times of strong (meridional flow) and weak (zonal flow) AL can successfully explain the variability at Jellybean, Marcella, and Mica Lakes. Meridional (zonal) flow causes high (low) $\delta^{18}O$ values at Mica Lake but low (high) $\delta^{18}O$ values at Jellybean Lake because the coastal setting of Mica Lake limits rain-out under meridional flow, while the interior setting of Jellybean Lake enhances rain-out. At Mica Lake, zonal flow is associated with Bering Sea moisture and rain-out over southwest Alaska, which is acknowledged by Anderson et al. (2007), whereas at Jellybean Lake, less rain-out occurs because direct flow against the St. Elias Mountains subsides.

Oxygen isotope values from an ice core ($\delta^{18}O_{ice}$) from the Mt. Logan summit (Fig. 3 inset) does not correlate with instrumental or paleo-temperature from the region (Holdsworth et al., 1992), although annual precipitation totals correlate with North Pacific climate indices (Moore et al., 2002). The $\delta^{18}O_{ice}$ values from Eclipse Icefield (Fig. 3 inset) is significantly correlated with northwestern North America temperature, but the correlation only explains between 5 and 10% of the variability (Wake et al., 2002). These results suggest site temperature is not the primary control of δP in the North Pacific.

Using an isotope model simulation, Fisher et al. (2004) suggest that isotope variability at Mt. Logan and Jellybean Lake can be explained by shifting moisture source. More specifically, two atmospheric flow regimes are prescribed for the model and provide a mechanism to explain changes in δP: under the mixed (meridional) flow regime, the moisture source includes low latitudes, whereas the zonal flow regime derives moisture strictly from the high latitudes of the North Pacific. The model predicts vertically stratified differences of δP between each flow regime. The difference between mixed and zonal regimes [$\delta^{18}O$ (zonal) – $\delta^{18}O$ (mixed)] above 1 km altitude is positive, and negative below 1 km. High-elevation sites receive relatively light δP under mixed flow while low-elevation sites receive heavy δP. The site response under different flow regimes would be opposite at Mica Lake (median catchment elevation = 364 m a.s.l.) compared to Jellybean Lake (effective catchment elevation = 1650 m a.s.l.) and Mt. Logan (5340 m a.s.l.). The suggestion that the altitudinal variability of δP in the North Pacific is best explained by changes in moisture source is consistent with the most plausible control at Mica Lake.

In general, the variability $\delta^{18}O$ values during early and mid-Holocene at Mica and Jellybean Lakes is lower than during the late Holocene (Fig. 17a and b). Mt. Logan $\delta^{18}O_{ice}$ does not show a late Holocene change to more variable values (Fig. 17c). The inverse relationship between $\delta^{18}O$ values at Mica Lake versus Jellybean Lake and Mt. Logan is not strongly evident and depends on the quality of the geochronology. However, the shift to more variable and lower $\delta^{18}O_{diatom}$ values at Mica Lake at 2.5 ka is coincident with generally increasing $\delta^{18}O$ values at both

Jellybean Lake and Mt. Logan, suggesting that moisture delivery shifted from zonal to meridional flow to all sites.

8.3. The Little Ice Age

The most recent shift to lower $\delta^{18}O_{diatom}$ values at Mica Lake coincides with the Little Ice Age (LIA), a time of global cooling (Grove, 2004). The LIA is well documented in the North Pacific region, enabling a detailed assessment of pan-North Pacific climate variability. Most south Alaska glaciers reached their Holocene maxima during the LIA (Wiles et al., 2007), suggesting that either summer temperature reached its minimum, or that winter precipitation was at its maximum, or both. Studies of glacier equilibrium-line altitudes find that lower summer temperatures and lower winter precipitation occurred during the LIA; the latter suggest a weaker AL (Daigle, 2006; McKay, 2007). Tree-ring records suggest that January to September temperatures in the Gulf of Alaska were reduced by about 1 ºC during the LIA (Wilson et al., 2007). These proxy records compare well with the low Mica Lake $\delta^{18}O_{diatom}$ values of 26.0 and 25.8‰ at 1820 and 1845 AD, respectively, which is interpreted as a period of weak AL, when south Alaska received proportionately more moisture from zonal flow.

8.4. The 20th century

Shifts of North Pacific climate are well documented during the 20th century, and provide a contemporary example of reorganization in the North Pacific that directly influenced south Alaska. The shift during the 1976-77 winter (Fig. 18) included a

deepening of the AL, pushing southward and strengthening storm tracks in the North Pacific (Miller et al., 1994). The 1976-77 shift is coincident with higher winter mass balance at Gulkana and Wolverine glaciers in south-central Alaska, but decreased winter mass balance at Cascade Glacier in Washington state, highlighting its broad impact on western North America (Hodge et al., 1998). Alaskan salmon production, which is dependent on marine productivity (Francis et al., 1998), has fluctuated at interdecadal timescales during the 20th century, coincident with North Pacific climate indices (Mantua et al., 1997). Similar 20th century shifts of Pacific climate occurred in 1925 and 1947 (Fig. 18), and define the PDO polarity reversals, which are positively correlated with the strength of the AL (Mantua et al., 1997). AL variability during the 20th century provides a contemporary example of its impact on storm-track trajectories intersecting south Alaska and its connection to other North Pacific climate indices.

During the 20th century, $\delta^{18}O_{diatom}$ values at Mica Lake show a monotonic increase (Fig 18). The top four contiguous MC-2 samples fall within the 20th century and the next youngest sample (1880 AD) is used to plot the trend from the 19th to 20th. Each sample represents about 15 yr of sedimentation (not accounting for any bioturbation), which is greater than the lake water residence time (< 5 yr). Therefore, each $\delta^{18}O_{diatom}$ value integrates multiple seasons of diatom blooms. The general increasing trend in $\delta^{18}O_{diatom}$ values contrasts with the 20th century winter NPI, which shows the multidecadal variability of the AL (Fig. 18). However, both time series have a first-order increasing trend over the 20th century. Sample resolution and bioturbation at Mica Lake smooth the influence of multidecadal

climate variability, and results in a centennial-scale record of changing δP, so the monotonic increase in $\delta^{18}O_{diatom}$ in spite of AL variability is understandable. Although the first-order trends further suggest the link between the AL and $\delta^{18}O_{diatom}$ values at Mica Lake, the small Mica Lake dataset limits a robust comparison.

9. Conclusions

The stable isotope ratios of water from south Alaska reveal a range of values across climate regimes. δW from lakes in maritime settings closely reflect δP, whereas water in interior lakes is strongly affected by evaporation. Water from lakes in the transitional climate setting are also influenced by evaporation, but are isotopically lighter due to colder temperatures at the higher-elevation sites sampled for this study. Multiple lines of evidence support the evaporation insensitivity of maritime lakes and the influence of evaporation at interior lakes, including 1) the δW values of maritime lakes define a slope parallel to the GMWL (8), whereas δW values from transitional and interior lakes have a lower slope (6), and 2) deuterium excess decreases from maritime to interior sites implying greater evaporation of lake water at interior sites. I found that δW at maritime lakes is more strongly correlated with median watershed elevation than with lake elevation, indicating that these lakes are good integrators of regional δP, not just δP over the lake site. Meteorological data from the climate station at Whittier suggest that the majority of precipitation falls during the winter months, when the atmospheric circulation is strongly influenced by the AL. Therefore, if regional δP is influenced by the strength and position of the

AL, δW will likely change as well. The paucity of long-term precipitation collections from south Alaska prevents a more robust test of this hypothesis, however.

A smaller survey of lake sediment in lakes of maritime PWS exhibits a $\delta^{18}O_{diatom}$ range larger than can be explained by temperature or the observed spatial variability of δW. The offset between the expected mean diatom age (last ~15 yr) and the age of the sampled water (few years) may partially explain the greater range in $\delta^{18}O_{diatom}$. Amplified (buffered) changes at high (low) elevation sites are also required to explain the increased slope between $\delta^{18}O_{diatom}$ and elevation compared to δW and elevation. Analyses of lake physiography reveal no reason for the greater change in $\delta^{18}O_{diatom}$ relative to lake water $\delta^{18}O$ at the site. A steeper vertical gradient of δP during the interval of time represented by $\delta^{18}O_{diatom}$ compared to the time represented by lake water $\delta^{18}O$ would cause the larger range of $\delta^{18}O_{diatom}$. Different or mixed sources of moisture between high (isotopically light) and low (isotopically heavy) sites is one mechanism that might explain the steep vertical δP gradient.

Both climatic and non-climatic factors influence $\delta^{18}O_{diatom}$. Previous studies have found enrichment of $\delta^{18}O_{diatom}$ due to dissolution during diagenesis. Little to no dissolution of diatoms and no downcore trend towards enriched $\delta^{18}O_{diatom}$ suggests that non-climatic factors are minimal. Low (0.4‰), intra-annual $\delta^{18}O$ of precipitation recorded at Adak suggests the seasonality of precipitation is not an important factor. I suggest that moisture source is the leading control, which seems most plausible considering the link between the AL and wintertime precipitation in south Alaska. Changes between meridional and zonal flow due to the changing

position and intensity of the AL would likely transport moisture from different sources. Under zonal flow conditions, south Alaska would receive isotopically light moisture because of greater rain-out and a colder source area (Bering Sea). South-to-north moisture transport over the Gulf of Alaska under meridional flow conditions would cause less rain-out and therefore be isotopically heavier.

I isolated diatoms from Holocene sediment from Mica Lake and measured their oxygen isotope ratios. The large variability of $\delta^{18}O_{diatom}$ values (4.6‰) from the 9600 yr record can be best explained by shifting moisture source although, realistically, $\delta^{18}O_{diatom}$ at Mica Lake integrates the effects of multiple controls. During the early to mid-Holocene (~9.6 to 2.5 ka) $\delta^{18}O_{diatom}$ values at Mica Lake are relatively high (28.6 ± 0.5 ‰) and stable. Since ~2.5 ka, brief, episodic decreases in $\delta^{18}O_{diatom}$ suggests variable atmospheric circulation, which might be linked to large-scale climate patterns in the tropical Pacific. The shift to decreasing lake productivity inferred from the OM and BSi at Mica Lake is coincident with the shift to more variable $\delta^{18}O_{diatom}$, corroborating a change of environmental conditions during the late Holocene. Low $\delta^{18}O_{diatom}$ values between ~1700-1900 AD coincide with the LIA, a time of global cooling, and glacier expansion in south Alaska. Similar times of lighter $\delta^{18}O_{diatom}$ occurred ~1.2 and 2.3 ka. Results from Mica Lake suggest that the AL was weaker and more moisture was carried by zonal flow during these times. During the 20th century, the NPI, a measure of the intensity of the AL, and $\delta^{18}O_{diatom}$, show first-order, increasing trends. The multidecadal variability of the AL, however, is likely smoothed in the Mica Lake $\delta^{18}O_{diatom}$ record due to low sample resolution.

δP paleorecords in the northern North Pacific show only weak correlations with air temperature (e.g., Holdsworth et al., 1992; Wake et al., 2002) or have $\delta^{18}O$ variations that are too great to be explained by changes in temperature (e.g., Anderson et al., 2005) and have been interpreted as "source meters" (Fisher et al., 2004). The large variability of $\delta^{18}O_{diatom}$ from evaporative-insensitive Mica Lake also suggests that moisture source has changed on centennial timescales. Viewed collectively, the growing number of δP paleorecords from the North Pacific emphasizes the variability of wintertime moisture delivery to northwestern North America as a pervasive feature of the regional climate.

10. Works Cited

Abell, P.I., Hoelzmann, P., 2000. Holocene palaeoclimates in northwestern Sudan: stable isotope studies on molluscs. Global and Planetary Change 26, 1-12.

Abbott, M.B., Wolfe, B.B., Aravena, R., Wolfe, W.P., Seltzer, G.O., 2000. Holocene hydrological reconstructions from stable isotopes and paleolimnology, Cordillera Real, Bolivia. Quaternary Science Reviews 19, 1801-1820.

Ager, T.A., 1998. Postglacial vegetation history of the Kachemak Bay Area, Cook Inlet, south-central Alaska. In: Kelley, K.D., Gough, L.P. (Eds.), Geologic Studies in Alaska by the US Geological Survey, 1998. US Geological Survey Professional Paper 1615, pp. 147–165.

Anderson, J., 2000. Diatoms, temperature, and climate. European Journal of Phycology 35, 307-314.

Anderson, L., Abbot, M.B., Finney, B.P., Burns, S., 2005. Regional atmospheric circulation change in the North Pacific during the Holocene inferred from lacustrine carbonate oxygen isotopes, Yukon Territory, Canada. Quaternary Research 64, 21-35.

Anderson, L., Abbott, M.B., Finney, B.P., Burns, S.J., 2007. Late Holocene moisture balance variability in the southwest Yukon Territory, Canada. Quaternary Science Reviews 26, 130-141.

Araguás-Araguás, L., Froehlich, K., Rozanski, K., 2000. Deuterium and oxygen-18 isotope composition of precipitation and atmospheric moisture. Hydrological Processes 14, 1341-1355.

Battarbee, R.W., Carvahlo, L., Juggins, S. Diatoms. In: Tracking Environmental Change Using Lake Sediments, Vol. 3: Terrestrial, Algal, and Siliceous Indicators, W. Last, J. Smol (Dordrecht, The Netherlands, Klumer, 2001), 155-202.

Beikman, H.M.,1980. Geologic map of Alaska; U.S. Geological Survey Professional Paper PP 0171, unpaged, 1 plate.

Bowen G.L., Ravenaugh, J., 2003. Interpolating the isotopic composition of modern meteoric precipitation. Water Resources Research 39, doi:10.1029/2003WR002086.

Bowen, G.J., Wilkinson, B., 2002. Spatial distribution of $\delta^{18}O$ in meteoric precipitation. Geology 30, 315-318.

Boyle, A.E., 1997. Cool tropical temperatures shift the global $\delta^{18}O$ -T relationship: An explanation for the ice core $\delta^{18}O$ – borehole thermometry conflict? Geophysical Research Letters 24, 273-276.

Brandriss, M.E., O'Neil, J.R., Edlund, M.B., Stoermer, E.F., 1998. Oxygen isotope fractionation between diatomaceous silica and water. Geochemica et Cosmochimica Acta 62, 1119–1125.

Cayan, D.R., Peterson, D.H., 1989. The influence of the North Pacific atmospheric circulation on streamflow in the west. Geophysical Monograph 55, 375-379.

Clague, J., Evans, S., Rampton, V., Woodsworth, G., 1995. Improved age estimates for the White River and Bridge River tephras, western Canada. Canadian Journal of Earth Sciences 32, 1172-1179.

Cockburn, J.M.H., Lamoureux, S.F., 2007. Century-scale variability in late-summer rainfall events recorded over seven centuries in subannually laminated lacustrine sediments, White Pass, British Columbia. Quaternary Research 67, 193-203.

Daigle, T., 2006. Late Holocene climate change at Goat Lake, Keni Mountains, south-central Alaska. M.S. Thesis, Flagstaff, AZ, Northern Arizona University, pp. 128.

Dansgaard, W., 1964. Stable isotopes in precipitation. Tellus 16, 436-468.

Denniston, R.F., González, L.A., Asmerom, Y., Baker, R.G., Reagan, M.K., Arthur Bettis. E., 1999. Evidence of increased cool season moisture during the middle Holocene. Geology 27, 815-818.

Desar, C., Phillips, A.S., Hurrell, J.W., 2004. Pacific interdecadal climate variability: linkages between the tropics and the North Pacific during boreal winter since 1900. Journal of Climate 17, 3109-3124.

Dodd, J.P, Sharp, Z.D., Fawcett, P.J., Schiff, C., Kaufman, D.S., 2007. A laser-extraction technique for oxygen isotope analysis of diatom frustules. EOS Transactions, American Geophysical Union, in press.

Fisher, D.A., Wake, C., Kreutz, K., Yalcin, K., Steig, R., Mayewski, P., Anderson, L., Zheng, J., Rupper, S., Zdanowicz, C., Demuth, M., Waszkiewicz, M., Dahl-Jensen, D., Goto-Azuma, K., Bourgeois, J.B., Koerner, R.M., Sekerka,

J., Osterberg, E., Abbott, M.B., Finney, B.P., 2004. Stable isotope records from Mount Logan, Eclipse ice cores and nearby Jellybean Lake. Water cycle of the North Pacific over 2000 years and over five vertical kilometers: sudden shifts and tropical connections. Géographie physique et Quaternaire 58, 9033-9048.

Francis, R.C., Hare, S.R., Hollowed, A.B., Wooster, W.S., 1998. Effects of interdecadal climate variability on the oceanic ecosystems of the NE Pacific. Fisheries Oceanography 7, 1-21.

Gat, J.R., 1981. Isotopic fractionation. In: Gat, J.R. and Gonfiantini, R., editors, Stable isotope hydrology, IAEA Technical Report Series 210, Vienna: International Atomic Energy Agency, 21–33.

Gibson, J.J., Edwards, T.W.D., Bursey, G.G., Prowse, T.D., 1993. Estimating evaporation using stable isotopes: Quantitative results and sensitivity analysis for two catchments in northern Canada. Nordic Hydrology 24, 79-94.

Grove, J., 2004. Little Ice Ages. Routledge, London, ed. 2nd, pp. 402.

Giese, B.S., Carton, J.A., 1999. Interannnual and decadal variability in the tropical and midlatitude Pacific Ocean. Journal of Climate 12, 3402-3418.

Heegaard, E., Birks, H.J.B., Telford, R.J., 2005. Relationships between calibrated ages and depth in stratigraphical sequences: an estimation procedure by mixed-effect regression. The Holocene 15, 612-618.

Hodge, S.M., Trabant, D.C., Krimmel, R.M., Heinrichs, T.A., March, R.S., Josberger, E.G., 1998. Climate variations and changes in mass of three glaciers in western North America. Journal of Climate 11, 2161-2179.

Holdsworth, G., Fogarasi, S., Krouse, H.R., 1991. Variation of the stable isotopes of water with altitude in the Saint Elias Mountains of Canada. Journal of Geophysical Research 96, 7483-7494.

Holdsworth, G., Krouse, H.R., Nosal, M., 1992. Ice core climate signals from Mount Logan, Yukon A.D. 1700–1897. In: Bradley, R.S., Jones, P.D. (Eds.), Climate Since A.D. 500. Routelidge, London, 483–516.

Hu, F.S., Ito, E., Brown, T.A., Curry, B.B., Engstrong, D.R., 2001. Pronounced climatic variations in Alaska during the last two millennia. Proceedings of the National Academy of Sciences 98, 10552-10556.

Hu., F.S., Shemesh, A., 2003. A biogenic-silica the last glacial-interglacial transition in southwester Alaska. Quaternary Research 59, 379-385.

Hu, F.S., Kaufman, D.S, Yoneji, S., Nelson, D., Shemesh, A., Huang, Y., Tian, J., Bond, G., Clegg, B., Brown, T., 2003. Cyclic variation and solar forcing of Holocene climate in the Alaskan subarctic. Science 301, 1890-1893.

Heusser, C.J., 1983. Holocene vegetation history of the Prince William Sound region, south-central Alaska. Quaternary Research 19, 337–355.

Juillet, A., 1980. Structure de la silice biogénique: nouvelles données apportees par l'analyse isotopique de l'oxygène. CR Academy of Science 290, 1237–1239.

Juillet-Leclerc, A., Labetrie, L., 1987. Temperature dependence of the oxygen isotopic fractionation between diatom silica and water. Earth and Planetary Science Letters 84, 69-74.

Kavanaugh, J.L., Cuffey, K.M., 2003. Space and time variation of $\delta^{18}O$ and δD of Antarctic precipitation revisited. Global Biogeochemical Cycles 17, doi:10.1029/2002GB001910.

Koutavas, A., deMenocal P.B., Olive, G.C., Lynch-Stieglitz, J., 2006. Mid-Holocene El Niño-Southern Oscillation (ENSO) attenuation revealed by individual foraminifera in eastern tropical Pacific sediments. Geology 34, 993-996.

Labeyrie, L.D., Juillet, A., Duplessy, J.C., 1984. Oxygen isotope stratigraphy: fossil diatoms vs foraminifera. In: Mann, D.G. (Ed.), Proceedings of the 7th International Symposium on Recent and Fossil Diatoms. Koeltz, Philadelphia, 477– 491.

Lamb, A.L., Leng, M.J., Sloane, H.J., Telford, R.J., 2005. A compariso of the palaeoclimate signals from diatom isotope ratios and carbonate oxygen isotope ratios from a low latitude crater lake. Palaeogeography, Palaeoclimatology, Palaeoecology 223, 290-302.

Leng, M.L., Marshall, J.D., 2004. Palaeoclimate interpretation of stable isotope data from lake sediment archives. Quaternary Science Reviews 23, 811-831.

Leng, M.L., Barker, P.A., 2006. A review of the oxygen isotope composition of lacustrine diatom silica for palaeoclimate reconstruction. Earth-Science Reviews 75, 5-27.

Locarnini, R.A., Mishonov, A.V., Antonov, J.I., Boyer, T.P., and Garcia, H.E., 2006. World Ocean Atlas 2005, Volume 1: Temperature. S. Levitus, Ed. NOAA Atlas NESDIS 61, U.S. Government Printing Office, Washington, D.C., 182 pp.

Mantua, N.J., Hare, S.R., Zhang, Y., Wallace, J.M., Francis, R.C., 1997. A Pacific interdecadal climate oscillation with impacts on salmon production. Bulletin of the American Meteorological Society 78, 1069-1079.

Masson-Delmotte, V., Jouzel, J., Landais, A., Stievenard, M., Johnsen, S.J., White, J.W.C., Werner, M., Sveinbjorndottir, A., Fuhrer, K., 2005. GRIP deuterium excess reveals rapid and orbital-scale changes in Greenland moisture origin. Science 309, 118-121.

McKay, N., 2007, Late Holocene climate at Hallet and Greyling Lakes, central Chugach Range, south-central Alaska. M.S. Thesis, Flagstaff, Arizona, Northern Arizona University, pp. 96.

Miller, A.J., Cayan, D.R., Barnett, T.P., Graham, N.E., Oberhuber, J.M., 1994. The 1976-77 climate shift of the Pacific Ocean. Oceanography 7, 21-26.

Moore, G.W.K., Holdsworth, G., Alverson, K., 2002. Climate change in the North Pacific region over the past three centuries. Nature 420, 401- 403.

Moore, G.W.K., Alverson, K., Holdsworth, G., 2003. The impact that elevation has on the ENSO signal in precipitation records from the Gulf of Alaska region. Climate Change 59, 101-121.

Morley, D.W., Leng, M.J., Mackay, A.W., Sloane, H.J., Rioual, P., Battarbee, R.W., 2004. Cleaning of lake sediment samples for diatom oxygen isotope analysis. Journal of Paleolimnology 31, 391-401.

Mortlock, R.A., Froelich, P.N., 1989. A simple method for the rapid determination of biogenic opal in pelagic marine sediments. Deep-Sea Research. Part A: Oceanographic Research Papers 36, 1415-1426.

Moschen, R., Lücke, A., Schleser, G.H., 2005. Sensitivity of biogenic silica oxygen isotopes to changes in surface water temperature and palaeoclimatology. Geophysical Research Letters 32, doi: 10.1029/2004GL022167.

Moschen, R., Lücke, A., Parples, J., Radtke, U., Schlesser, G.H., 2006. Transfer and early diagenesis of biogenic silica oxygen isotope signals during settling and sedimentation of diatoms in a temperate freshwater lake (Lake Holzmaar, Germany). Geochemica et Cosmochimica Acta 70, 4367-4379.

Moy, C.M., Seltzer, G.O., Rodbell, D.T., Anderson, D.M., 2002. Variability of El Niño/Southern Oscillation activity at millennial time scales during the Holocene epoch. Nature 420, 162-165.

Nesje, A., Dahl, S.O. 2001. The Greenland 8200 cal. yr BP event detected in loss-on-ignition profiles in Norwegian lacustrine sediment sequences. Journal of Quaternary Science 16, 155-66.

Nesje, A., Dahl, S.O., Lie, Ø., 2004. Holocene millennial-scale summer temperature variability inferred from sediment parameters in a non-glacial mountain lake: Danntjørn, Jotunheimen, central southern Norway. Quaternary Science Reviews 23, 2183-205.

Nesje, A., Bakke, J., Dahl, S.O., Lie, Ø., Bøe, A., 2007. A continuous, high-resolution 8500-yr snow-avalanche record from western Norway. The Holocene 17, 269-277.

Newman, J.E., Branton, C.I., 1972. Annual water balance and agricultural development in Alaska. Ecology 53, 519-519.

Overland, J.E., Adams, J.M., Bond, N.A., 1999. Decadal variability of the Aleutian Low and its relation to high-latitude circulation. Journal of Climate 12, 1542-1548.

Papineau, J.M., 2001. Wintertime temperature anomalies in Alaska correlated with ENSO and PDO. International Journal of Climatology 21, 1577-1592.

Pinglot, J.F., Pourchet, M., 1995. Radioactivity measurements applied to glaciers and lake sediments. The Science of the Total Environment 173/174, 211–223.

Reimer, P.J., Baillie, M.G.L., Bard, E., Bayliss, A., Beck, J.W., Bertrand, C.J.H., Blackwell, P.G., Buck, C.E., Burr, G.S., Cutler, K.B., Damon, P.E., Edwards, R.L., Fairbanks, R.G., Friedrich, M., Guilderson, T.P., Hogg, A.G., Hughen, K.A., Kromer, B., McCormac, G., Manning, S., Ramsey, C.B., Reimer, R.W., Remmele, S., Southon, J.R., Stuiver, M., Talamo, S., Taylor, F.W., van der Plicht, J., Weyhenmeyer, C.E., 2004. INTCAL04 terrestrial radiocarbon age calibration, 0-26 cal kyr BP. Radiocarbon 46, 1029-1058.

Rings, A., Lücke, A., Schleser, G.H., 2004. A new method for the quantitative separation of diatom frustules from lake sediments. Limnology and Oceanography: Methods 2, 25-34.

Rodionov, S.N., Overland, J.E., Bond., N.A., 2005. Spatial and temporal variability of the Aleutian Climate. Fisheries Oceanography 14, 3-21.

Rosqvist, G., Jonsson, C., Yam., R., Karlén, W., Shemesh A., 2004. Diatom oxygen isotopes in pro-glacial lake sediments from northern Sweden: a 5000 year record of atmospheric circulation. Quaternary Science Reviews 23, 851-859.

Round, F.E., Crawford, R.M., Mann, D.G., 1990. The diatoms: Biology and morphology of the genera: Cambridge, UK, Cambridge University Press, pp. 747.

Rozanski, K., Araguás-Araguás, L., Gonfiantini, R., 1993. Isotopic patterns in modern global precipitation. In: Swart, P. K., Lohmann, K.C., McKenzie, J. and Savin, S. (eds), Climate Change in Continental Isotopic Records. Geophysical Monograph 78. American Geophysical Union, Washington, D.C., 1–36.

Rupper, S., Steig, E.J., Roe, G., 2004. The relationship between snow accumulation at Mt. Logan, Yukon, Canada, and climate variability in the North Pacific. Journal of Climate 17, 4724-4739.

Salathé, E.P., 2006. Influences of a shift in North Pacific storm tracks on western North American precipitation under global warming. Geophysical Research Letters 33, doi:10.1029/2006GL026882.

Sauer, P.E., Miller, G.H., Overpeck, J.T., 2001. Oxygen isotope ratios of organic matter in arctic lakes as a paleoclimate proxy: field and laboratory investigations. Journal of Palelimnology 25, 43-64.

Schiff, C.S., Kaufman, D.S., Wallace, K.L., Werner, A., Ku, R., Brown, T.A., 2008. Modeled tephra ages from lake sediments, base of Redoubt Volcano, Alaska. Quaternary Geochronology 3, 56-67.

Schmidt, M., Botz, R., Stoffers, P., Anders, T., Bohrman, G., 1997. Oxygen isotopes in marine diatoms: A comparative study of analytical techniques and new

results on the isotope composition of recent marine diatoms. Geochimica et Cosmochimica Acta 61, 2275-2280.

Schmidt, M., Botz, R., Rickert, D., Bohrman, G., Hall, S.R., Mann, S., 2001. Oxygen isotopes of marine diatoms and relations to opal-A maturation. Geochimica et Cosmochimica 65, 201-211.

Seierstad, J., Nesje, A., Dahl, S.O., Simonsen, J.R., 2002. Holocene glacier fluctuations of Grovabreen and Holocene snow-avalanche activity reconstructed from lake sediments in Grøningstølsvatnet, western Norway. The Holocene 12, 211-222.

Shemesh, A., Peteet, D., 1998. Oxygen isotopes in fresh water biogenic opal – Northeastern US Alleröd-Younger Dryas temperature shift. Geophysical Research Letters 25, 1935-1938.

Shemesh, A., Charles, C.D., Fairbanks, R.G., 1992. Oxygen isotopes in biogenic silica: global changes in ocean temperature and isotopic composition. Science 256, 1434-1437.

Shemesh, A., Rosqvist, G., Rietti-Shati, M., Rubensdotter, L., Bigler, C., Yam, R., Karlén, W., 2001. Holocene climatic change in Swedish Lapland inferred from an oxygen-isotope record of lacustrine biogenic silica. The Holocene 11, 447-454.

Spooner, I.S., Mazzucchi, D., Osborn, G., Gilbert, R., Larocque, I., 2002. A multi-proxy Holocene record of environmental change from the sediments of Skinny Lake, Iskut region, northern British Coumbia, Canada. Journal of Paleolimnology 28, 419-431.

Spooner, I.S., Barnes, S., Baltzer, K.B., Raeside, R., Osborn, G.D., Mazzuchi, D., 2003. The impact of air mass circulation dynamics on Late Holocene paleoclimate in northwestern North America. Quaternary International 108, 77-83.

Stenni, B., Masson-Delmotte, V., Johnsen, S., Jouzel, J., Longinelli, A., Monnin, E., Roethlisberger, R. Selmo, E., 2001. An oceanic cold reversal during the last deglaciation. Science 293, 2074–2077.

Stuiver, M., Polach, H.A., 1977. Discussion: reporting of ^{14}C data. Radiocarbon 19, 355–363.

Stuiver, M., Reimer, P.J., 1993. Extended ^{14}C database and revised CALIB 3.0 ^{14}C calibration program. Radiocarbon 35, 215–230.

Telford, R.J., Heegaard, E., Birks, H.J.B., 2004. The intercept is a poor estimate of a calibrated radiocarbon age. The Holocene 14 296-298.

Terranes, J.L., McKenzie, J.A., 2001. Lacustrine oxygen isotope record of 20th-century climate change in central Europe: evaluation of climatic controls on oxygen isotopes in precipitaiton. Journal of Paleolimnology 26, 131-146.

Trenberth, K.E., Hurrell, J.W., 1994. Decadal atmospere-ocean variations in the Pacific. Climate Dynamics 9, 303-319.

Vose, R.S., Schmoyer, R.L., Steurer, P.M., Peterson, T.C., Heim, R., Karl, T.R., Eischeid, J.K., 1992. The Global Historical Climatology Network; Long-Term Monthly Temperature, Precipitation, Sea Level Pressure, and Station Pressure Data. ORNL/CDIAC-53, NDP-041. Available on-line [http://cdiac.esd.ornl.gov/epubs/ndp/ndp041/ndp041.html] from Carbon

Dioxide Information Analysis Center (CDIAC), Oak Ridge National Laboratory, Oak Ridge, Tennessee, U.S.A.

Wake, C.P., Yalcin, K., Gundestrup, N.S., 2002. The climate signal recorded in the oxygen-isotope, accumulation and major-ion time series from the Eclipse ice core, Yukon Territory, Canada. Annals of Glaciology 35, 416–422.

White, W.B., Walker, A.E., 1973. Meridional atmospheric teleconnections over the North Pacific from 1950 to 1972. Monthly Weather Review 101, 817-822.

Wiles, G.C., Barclay, D.J., Calkin, P.E., Lowell, T.V., 2007. Century to millennial-scale temperature variations for the last two thousand years indicated from glacial geologic records of Southern Alaska. Global and Planetary Change, in press.

Wilson, R., Wiles, G., D'Arrigo, R., Zweck, C., 2007. Cycles and shifts: 1,300 years of multi-decadal temperature variability in the Gulf of Alaska. Climate Dynamics 28, 425-440.

Wooller, M.J., Francis, D., Fogel, M.L., Miller, G.H., Walker, I.R., Wolfe, A.P., 2004. Quantitative paleotemperature estimates from $\delta^{18}O$ of chironomid head capsules preserved in arctic lake sediments. Journal of Paleolimnology 31, 267-274.

Wooller, M., Wang, Y., Axford, Y., in prep. A multiple stable isotope record of Late Quaternary limnological changes and chironomid paleoecology from northeastern Iceland. Journal of Paleolimnology.

Yin, J.H., 2005. A consistent poleward shift of the storm tracks in simulations of 21st century climate. Geophysical Research Letters 32, doi:10.1029/2005GL023684.

Yurtsever, Y., Gat, J.R. 1981. Atmospheric waters. In: Gat, J.R. and Gonfiantini, R., editors, Stable isotope hydrology, IAEA Technical Report Series 210, Vienna: International Atomic Energy Agency, 103–142.

Table 1 Expression of the Aleutian Low in the eastern North Pacific

Aleutian Low intensity	Strong	Weak
Gulf of Alaska winter surface air temperature	warm	cool
Gulf of Alaska winter precipitation	high	low
Gulf of Alaska sea surface temperature	warm	cool
North Pacific storm track trajectory	southerly	northerly or westerly
Moisture transport	meridional	zonal

Table 2 Climate station site and summary data

Station name:	Latitude (°N)	Longitude (°W)	Elevation (m)	Mean air temperature (°C)	Annual precipitation (mm)
			PWS/maritime		
Cannery Creek	61.02	147.52	3	3.6	3110
Cordova	60.50	145.50	15	4.4	2440
Seward	60.12	149.45	24	4.8	1750
Whittier	60.78	148.68	18	5.2	5480
Valdez	61.13	146.35	6	3.9	1810
Adak	51.88	176.65	4	4.8	1680
			Interior		
Gulkana	62.15	145.45	482	-2.1	280
Snowshoe Lake	62.03	146.67	701	-4.9	250
Tonsina	61.65	145.17	457	-2.7	270

Table 3 Location, water depth, length, and notes for cores from Mica Lake

Core ID	Latitude (°N)	Longitude (°W)	Water depth (m)	Core length (m)	Corer type	Notes
MC-1	60.3615	148.1490	44	1.3	Percussion	
MC-1-A	60.3615	148.1490	44	0.2	Gravity	Sub-sampled in field
MC-2	60.6741	148.1359	58	3.1	Percussion	
MC-2-A	60.6741	148.1359	58	0.2	Gravity	Sub-sampled in field
MC-2-B	60.6741	148.1359	58	0.2	Gravity	
MC-2-C	60.6741	148.1359	58	0.3	Gravity	Split in field
MC-3	60.6832	148.1380	49	1.7	Percussion	
MC-3-A	60.6832	148.1380	49	0.2	Gravity	Split in field

Table 4 Characteristics and surface-water isotope values for surveyed lakes located within 210 km of Mica Lake

Site name/code[a]	Collection date	Latitude (°N)	Longitude (°W)	Elevation (m)	Climate zone[b]	Lake type	Topographic setting[c]	$\delta^{18}O$ (‰)	δD (‰)
Robe	Aug-2007	61.085	146.172	9	Maritime	Non-glacial	Open	-15.9	-127
Shrode	Jun-2006	60.652	148.330	24	Maritime	Non-glacial	Open	-14.0	-99
Turner	Jun-2006	60.910	146.627	33	Maritime	Non-glacial	Open	-14.4	-107
Portage	Aug-2007	60.846	148.987	54	Maritime	Glacial	Open	-14.9	-112
Miners	Jun-2006	61.079	147.436	55	Maritime	Glacial	Open	-16.4	-123
Milliard	Jun-2006	60.906	146.578	80	Maritime	Non-glacial	Open	-15.3	-113
Silver	Jun-2006	60.930	146.462	95	Maritime	Glacial	Open	-15.6	-116
"Mica"	Jun-2006	60.692	148.149	100	Maritime	Non-glacial	Open	-12.9	-98
"Mica pond"	Aug-2007	60.694	148.148	103	Maritime	Non-glacial	Closed	-8.6	-63
Bear (Seward Pen)	Aug-2007	60.191	149.358	111	Maritime	Glacial	Open	-14.4	-111
"Cascades"	Jun-2006	60.930	147.869	180	Maritime	Glacial	Open	-14.8	-108
Trail	Aug-2007	60.489	149.368	180	Maritime	Glacial	Open	-17.2	-134
Tern	Aug-2007	60.535	149.545	221	Maritime	Non-glacial	Open	-16.5	-128
Lower Paradise	Jun-2006	60.344	149.074	290	Maritime	Non-glacial	Open	-16.0	-120
Jerome	Aug-2007	60.546	149.570	300	Maritime	Non-glacial	Closed	-15.6	-128
Nellie Juan	Jun-2006	60.248	149.045	350	Maritime	Glacial	Open	-15.9	-117
"Allison"	Jul-2006	61.040	146.349	413	Maritime	Glacial	Open	-16.7	-124
Summit	Aug-2007	60.636	149.504	435	Maritime	Non-glacial	Open	-17.5	-134
Willow	Aug-2007	61.787	145.184	435	Interior	Non-glacial	Closed	-13.3	-129
Long	Aug-2007	61.805	148.234	468	Interior	Non-glacial	Closed	-13.9	-128
"GRS-1"	Aug-2007	62.106	145.471	470	Interior	Non-glacial	Closed	-16.8	-151
"GRS-2"	Aug-2007	61.522	145.226	570	Transitional	Non-glacial	Closed	-15.0	-138
Blueberry	Aug-2007	61.121	145.697	610	Transitional	Non-glacial	Closed	-17.2	-136
Pippin	Aug-2007	61.714	145.161	621	Interior	Non-glacial	Closed	-13.0	-128
Plumbob	Aug-2007	62.107	145.945	624	Interior	Non-glacial	Closed	-14.8	-134
Tolsona	Aug-2007	62.109	146.037	630	Interior	Non-glacial	Open	-13.5	-131
"Ptarmigan"	Aug-2007	61.148	145.723	705	Transitional	Non-glacial	Closed	-18.5	-139
"Lee"	Jul-2006	62.085	146.395	760	Interior	Non-glacial	Closed	-16.1	-143
"Goat"	Jul-2006	60.260	149.905	840	Maritime	Non-glacial	Open	-15.9	-123
Greyling	Jul-2006	61.392	145.736	1000	Transitional	Glacial	Open	-20.6	-154
"Eureka"	Aug-2007	61.939	147.168	1010	Interior	Non-glacial	Closed	-15.7	-138
"Hallet"	Jul-2006	61.494	146.238	1160	Transitional	Glacial	Open	-21.5	-160

[a] " " indicates informal name. [b]Papinaeua, 2001. [c]Topographic setting closed = no surface outflow

Table 5 Correlation matrix for PWS lake and watershed characteristics

	Lake area	Watershed area	Watershed/lake area	Lake elevation	Median watershed elevation	$\delta^{18}O$	δD
Lake area		0.62[b]	-0.19	-0.31	0.16	-0.22	-0.25
Watershed area	*0.86* [a]		0.58[b]	-0.10	0.42	-0.62	-0.30
Watershed/lake area	*0.63* [b]	*0.89* [a]		0.03	0.41	-0.32	-0.22
Lake elevation	*-0.14*	*-0.09*	*-0.20*		0.65	-0.60[a]	-0.59[a]
Median watershed elevation	*0.62*	*0.42*	*0.35*	*0.38*		-0.95[b]	-0.90[b]
$\delta^{18}O$	*-0.44*	*-0.42*	*-0.61*	*-0.39*	*-0.60*		0.96[b]
δD	*-0.58*	*-0.74*	*-0.65*	*-0.21*	*-0.40*	*0.98* [b]	

Note: Statistics in *italics* are from glacial lake data.
[a]Significant at the 99% confidence level.
[b]Significant ath the 90% confidence level.

Table 6 Core top and trap diatom and lake-water isotope values

Climate zone[a]	Lake[b]	$\delta^{18}O$ (‰)			Projected temperature (ºC)	
		water	diatom[c]	Δ[d]	Mean annual	Summer (JJA)
Interior	"Lee"	-16.07	26.90	42.97	-2.4	12.8
Maritime	"Goat"	-15.90	22.72	38.62	4.2	12.2
Maritime	"Mica"	-12.92	29.80	42.72	5.1	13.4
Maritime	Shrode	-14.04	26.68	40.72	5.1	13.5
Maritime	Milliard	-15.28	24.66	39.94	4.4	12.0

[a]Papineaua, 2001.
[b] " " indicates informal name.
[c]Diatoms recovered from lakes are from top sediment except for "Lee Lake", where diatoms were collected in traps between July 2005 and July 2006.
[d]$\Delta = \delta^{18}O_{diatom}$ – lake water $\delta^{18}O$

Table 7 ^{210}Pb and ^{137}Cs activity of gravity cores MC-2-A and -C

Depth blf (cm)[a]	$^{210}Pb_{ex}$ (dpm/g)	^{137}Cs (dpm/g)
	MC-2-A	
0.125	4.7 ± 0.08	11.69 ± 0.27
0.625	3.5 ± 0.20	6.27 ± 0.32
1.125	2.74 ± 0.29	4.33 ± 0.28
2.125	2.47 ± 0.30	4.35 ± 0.26
3.125	2.62 ± 0.25	3.36 ± 0.23
4.125	2.57 ± 0.13	2.90 ± 0.12
	MC-2-C	
0.25	2.92 ± 0.24	4.58 ± 0.27
0.75	2.31 ± 0.36	4.20 ± 0.27
1.25	2.08 ± 0.32	1.39 ± 0.24
1.75	2.04 ± 0.42	2.69 ± 0.26
2.25	2.36 ± 0.25	1.63 ± 0.19
2.75	2.73 ± 0.40	1.01 ± 0.40
3.25	-0.84 ± -2.03	0.62 ± 0.14
3.75	-0.49 ± -1.48	0.49 ± 0.30

Note: data from R. Ku and V. Todd, University of Southern California.

[a]Centered sample depth. Sample thicknesses are 0.25 cm and 0.50 cm for MC-2-A and MC-2-C, respectively.

Table 8 Radiocarbon and calibrated ages from core MC-2

Depth blf (cm)[a]	^{14}C age (yr BP)	Calibrated age (cal yr)[b]	Dated material[c]	Lab ID
4.25	285 ± 15	380 ± 60	Wood	29509[d]
24.50[f]	1350 ± 15	1290 ± 5	Hemlock needles	29510[d]
25.25[f]	1180 ± 20	1110 ± 55	Hemlock needles	134202[e]
24.00[f]	1500 ± 35	1380 ± 35	Mixed macrofossils	134203[e]
26.00	1200 ± 40	1125 ± 55	Hemlock needles	33147[d]
36.00	1390 ± 20	1300 ± 10	Hemlock needles	29511[d]
54.25	1565 ± 15	1470 ± 50	Mixed macrofossils	134204[e]
55.00	1655 ± 40	1555 ± 85	Hemlock needlese	33148[d]
65.00	2040 ± 60	2010 ± 90	Aquatic moss	134205[e]
74.75	2390 ± 70	2460 ± 170	Mixed macrofossils	134206[e]
85.00	2790 ± 70	2900 ± 85	Aquatic moss	134207[e]
133.50	3580 ± 15	3880 ± 25	Bark	29512[d]
149.75	4135 ± 20	4680 ± 110	Hemlock needlese	33149[d]
177.50[f]	5975 ± 25	6815 ± 50	Bark	29513[d]
188.25	5135 ± 20	5910 ± 10	Aquatic moss	33150[d]
276.75	8500 ± 60	9500 ± 30	Mixed macrofossils	34298[d]

^{14}C ages were calculated following the conventions of Stuiver and Polach (1977).

[a]Centered sample depth; samples 0.25 - 0.5 cm thick.

[b]Median probability ± one-half of 1σ age range from CALIB v.5.0.2 (Stuiver and Reimer, 1993).

[c]Mixed macrofossils include various proportions of aquatic moss, Hemlock needles, wood, and leaf fragments.

[d]Lawrence Livermore National Laboratory, Center for Accelerator Mass Spectrometry (CAMS).

[e]Keck Carbon Cycle AMS Facility, University of California Irvine (UCIAMS).

[f]Excluded from age model.

Table 9 List of tephra data from core MC-2

Tephra ID	Centered tube depth (cm)	Thickness (cm)	Model age (yr BP)
1	10.25	2.5	390
2	35.25	1.5	1040
3	144.75	0.5	3950
4	203.00	2.0	5630
5	223.50	1.0	6485
6	311.00	1.0	9985

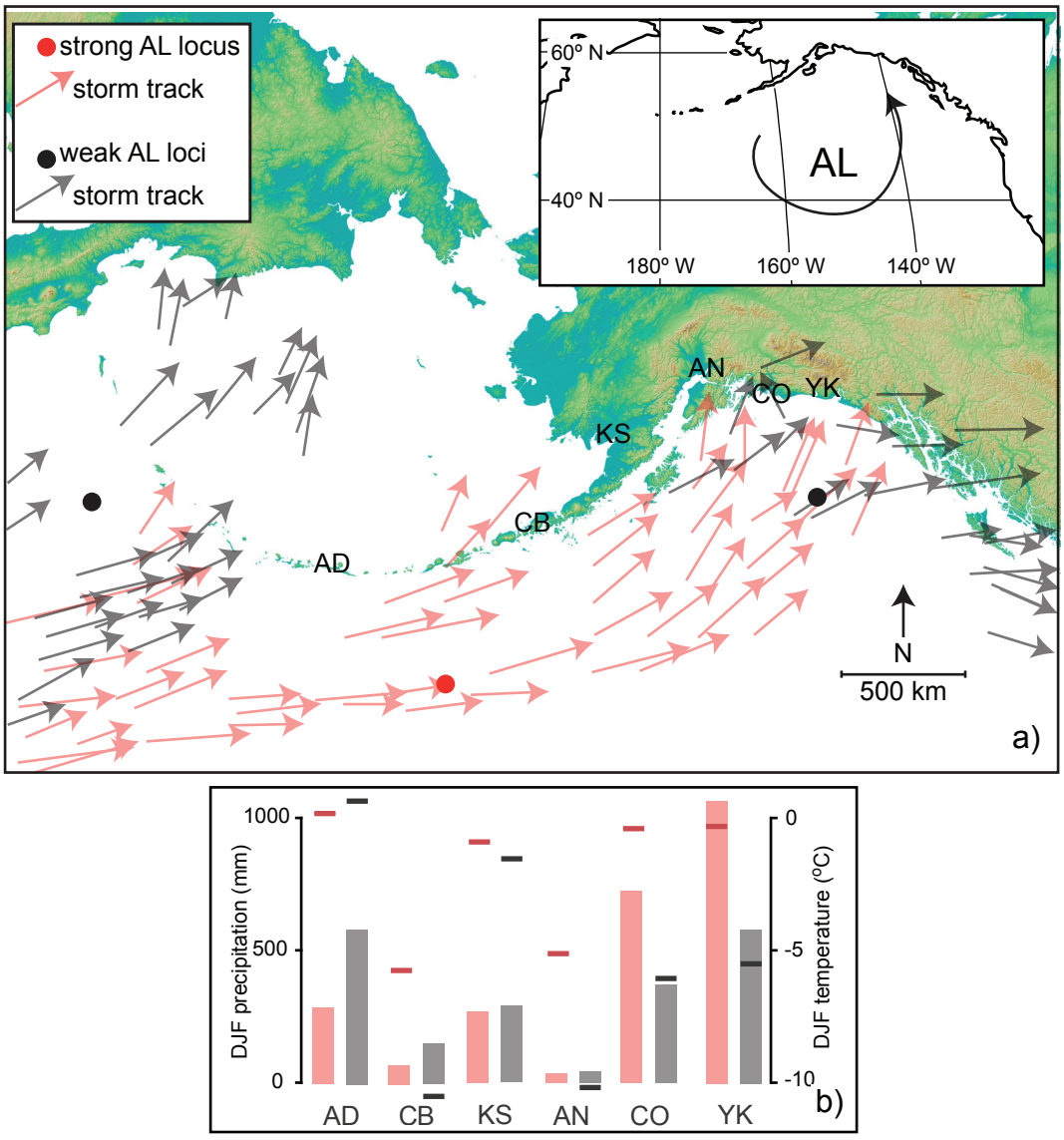

Fig. 1 (a) Comparison of the wintertime (DJF) Aleutian Low (AL) during the 10 strongest (red) versus the 10 weakest (black) years between 1951 and 2000 as summarized by Rodionov et al. (2005). (b) Summary of meteorological observations during the ten strongest and weakest AL years at Adak (AD), Cold Bay (CB), King Salmon (KS), Anchorage (AN), Cordova (CO), and Yakutat (YK), displayed from left to right, respectively. Total DJF precipitation amounts are vertical bars, and average DJF temperatures are thick lines. In general, eastern sites record higher winter (DJF) precipitation and temperatures during strong AL years. Precipitation amounts at Adak and Cold Bay are inversely related to eastern sites (Cordova and Yakutat). Precipitation amounts at King Salmon and Anchorage are nearly identical between strong and weak AL years. Adak temperatures are inversely related to all other sites, although the difference between strong and weak years is small (1.2 °C). Climate data obtained from the Global Historic Climate Network (Vose et al., 1992).

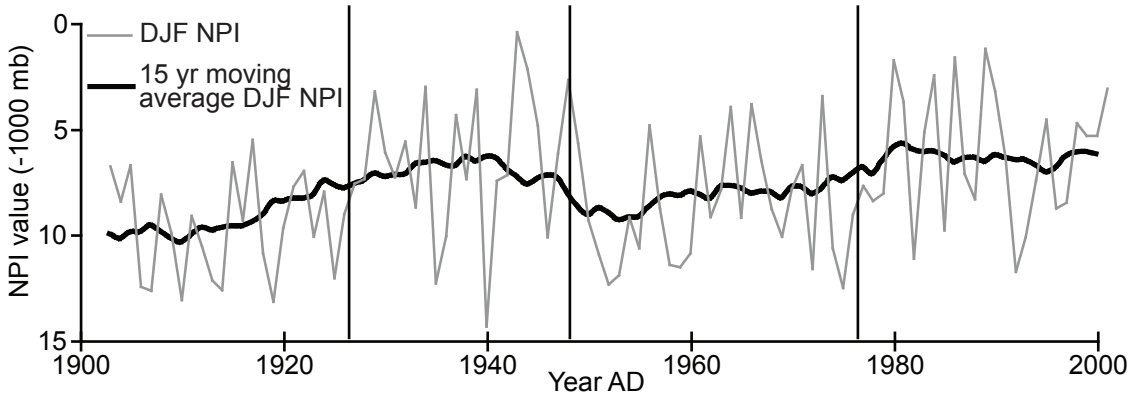

Fig. 2 The annual and 15 yr moving average DJF North Pacific Index (NPI) (see text for details), which is a measure of the intensity of the Aleutian Low (AL). High NPI values correspond to weak AL. Black vertical bars mark the three shifts of the NPI during the 20th century at 1925, 1947, and 1976. NPI data provided by the Climate Analysis Section, NCAR, Boulder, USA, Trenberth and Hurrell (1994).

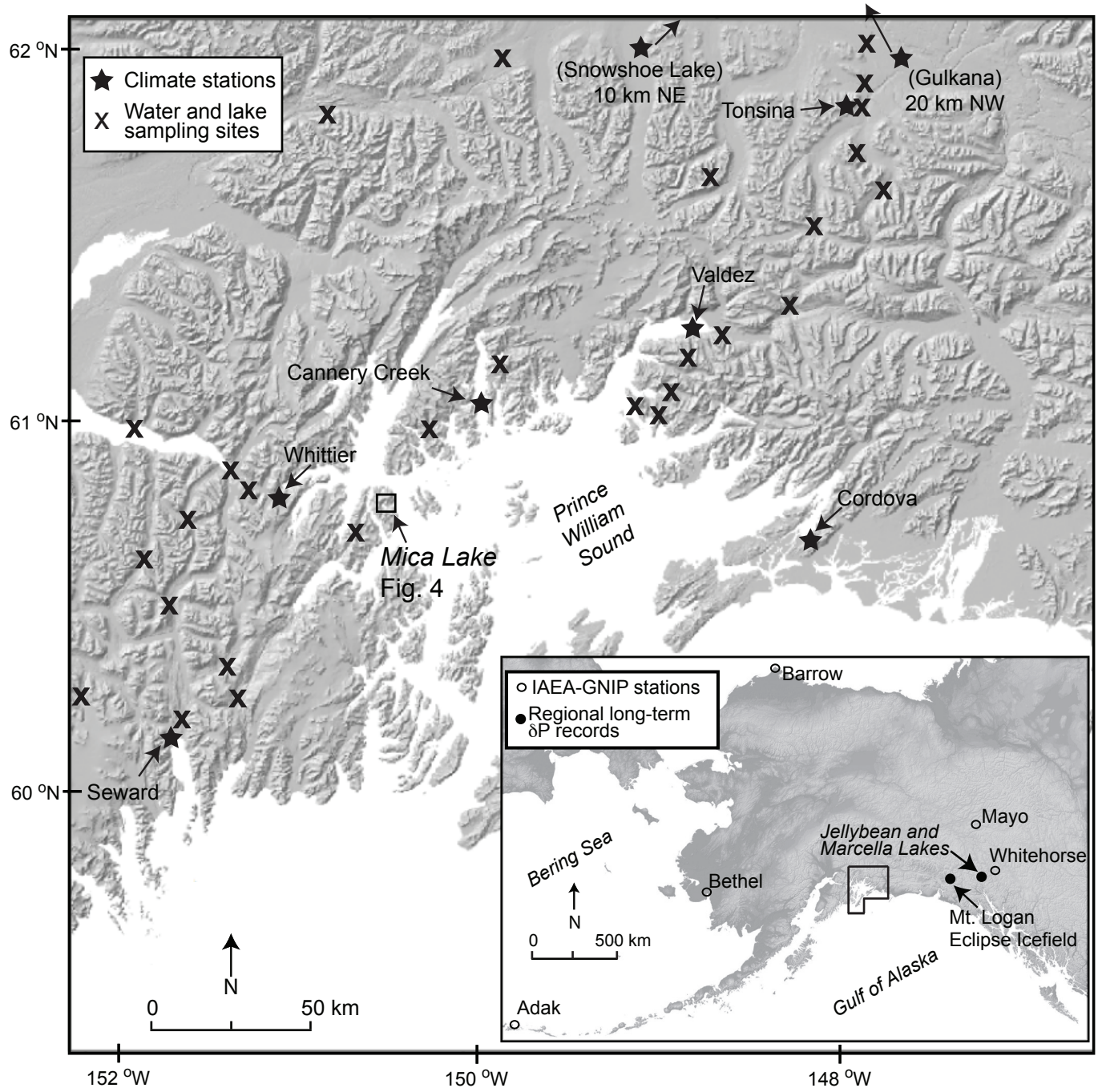

Fig. 3 Study area with water sampling sites (x), climate stations (★), North Pacific International Atomic Energy Agency-Global Network of Isotopes in Precipitation (IAEA-GNIP) stations (●), locations of North Pacific paleorecords of stable isotopes of precipitation (δP) (○), and Mica Lake.

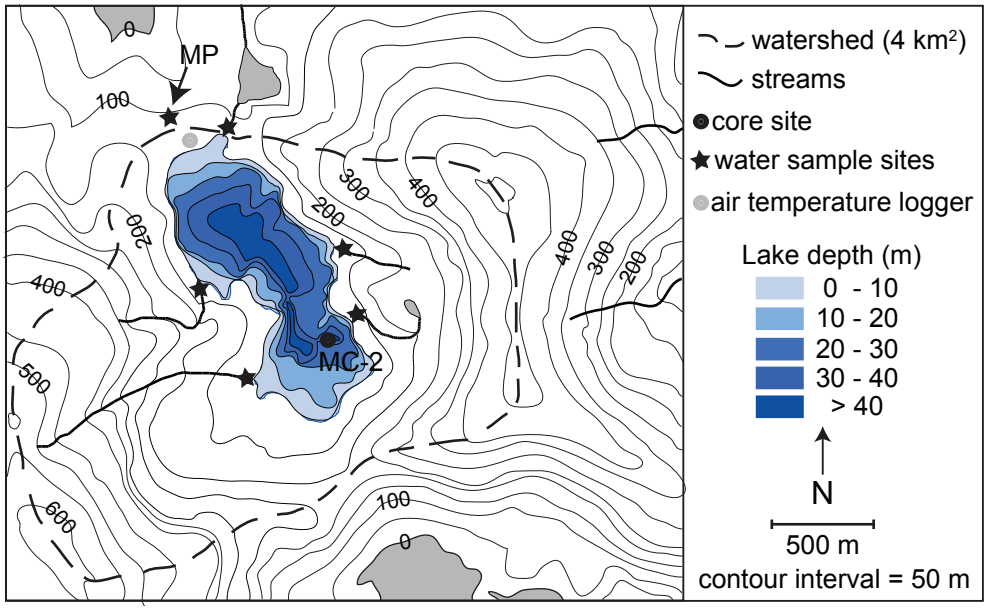

Fig. 4 Mica Lake watershed (dashed line) and bathymetry, with coring (●) and water sampling (★) sites. "MP" refers to Mica Pond (see text for details). Map location is shown in Fig. 3.

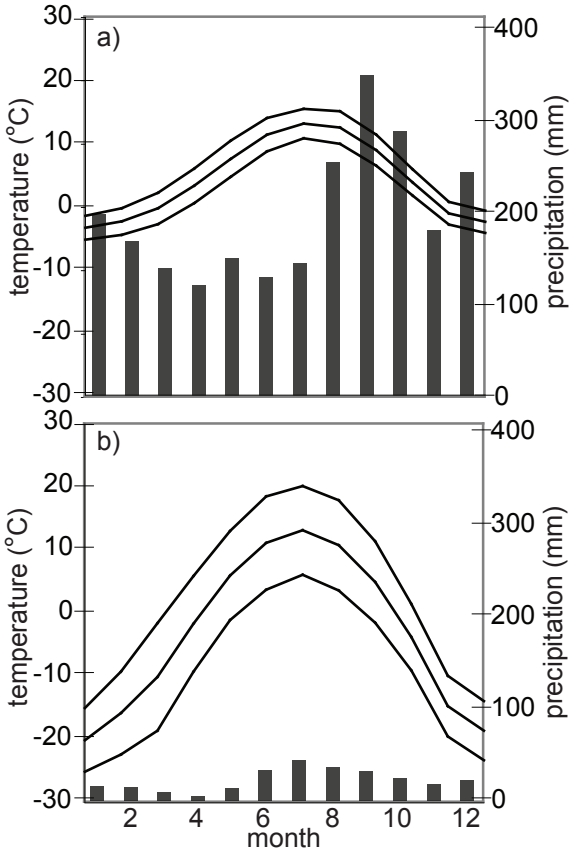

Fig. 5 Monthly maximum, mean, and minimum temperatures (solid lines), and precipitation (vertical bars) from five long-term climate stations around (a) Prince William Sound and (b) three interior stations between 1980 and 2005. Both climate summaries are plotted on equivalent axes. See text, Table 2, and Fig. 3 for climate station locations and explanation of data treatment.

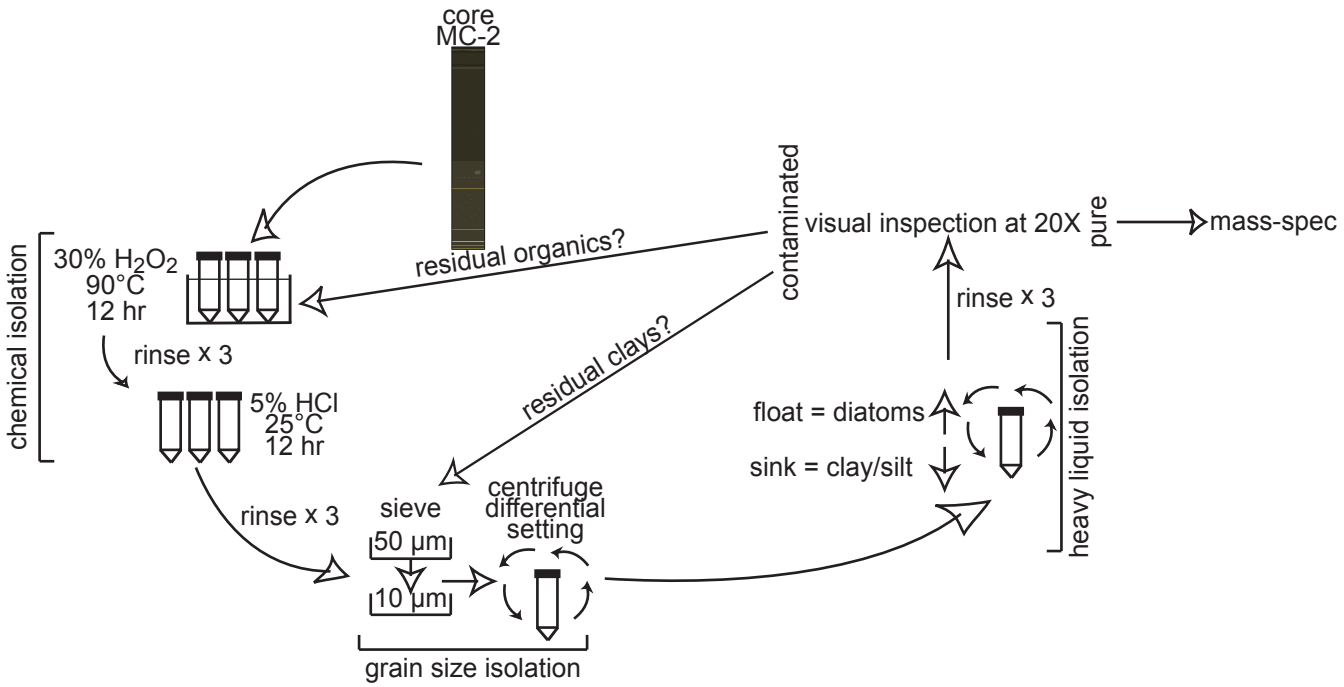

Fig. 6 Flow chart illustrating the diatom isolation protocol adapted from Morley et al. (2004).

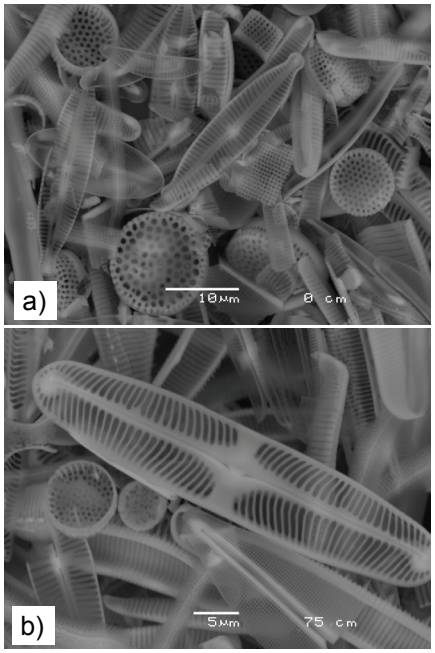

Fig. 7 Backscattered electron microscope image of purified diatom samples from (a) 0 cm and (b) 75 cm depth blf from core MC-2.

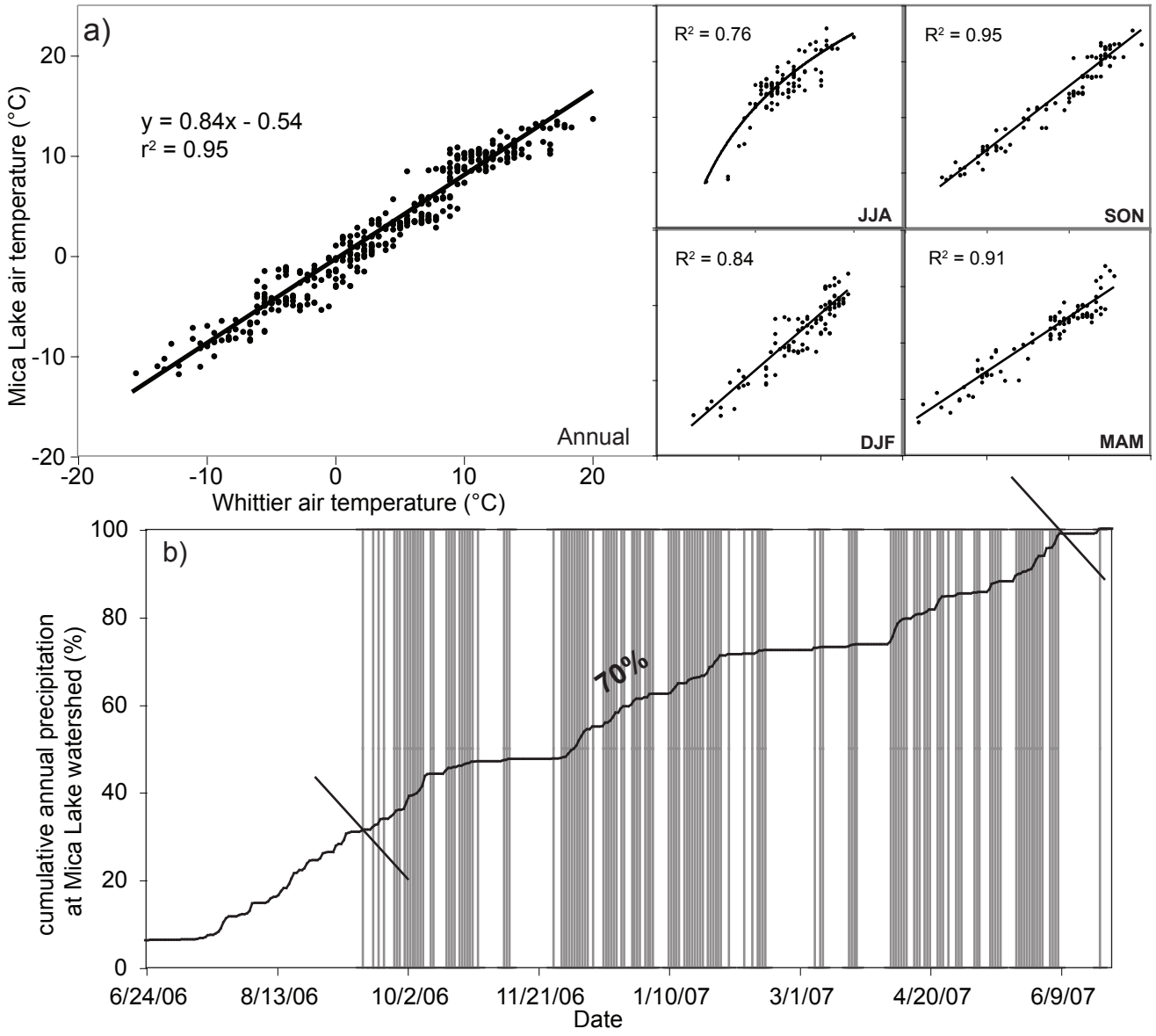

Fig. 8 (a) Daily air temperature at Mica Lake compared to Whittier, AK between 3 July 2006 and 2 July 2007. Data were subdivided to calculate seasonal lapse rates used to estimate temperature at the median elevation of the Mica Lake watershed (364 m a.s.l.). Black lines are least-squares linear or power (JJA) regressions. Data available online: http://jan.nau.ucc.edu/~dsk5/S_AK/. (b) Cumulative precipitation (black line) with the days of below 0 °C daily temperatures at the median elevation of the Mica Lake watershed and precipitation received at Whittier (vertical gray lines).

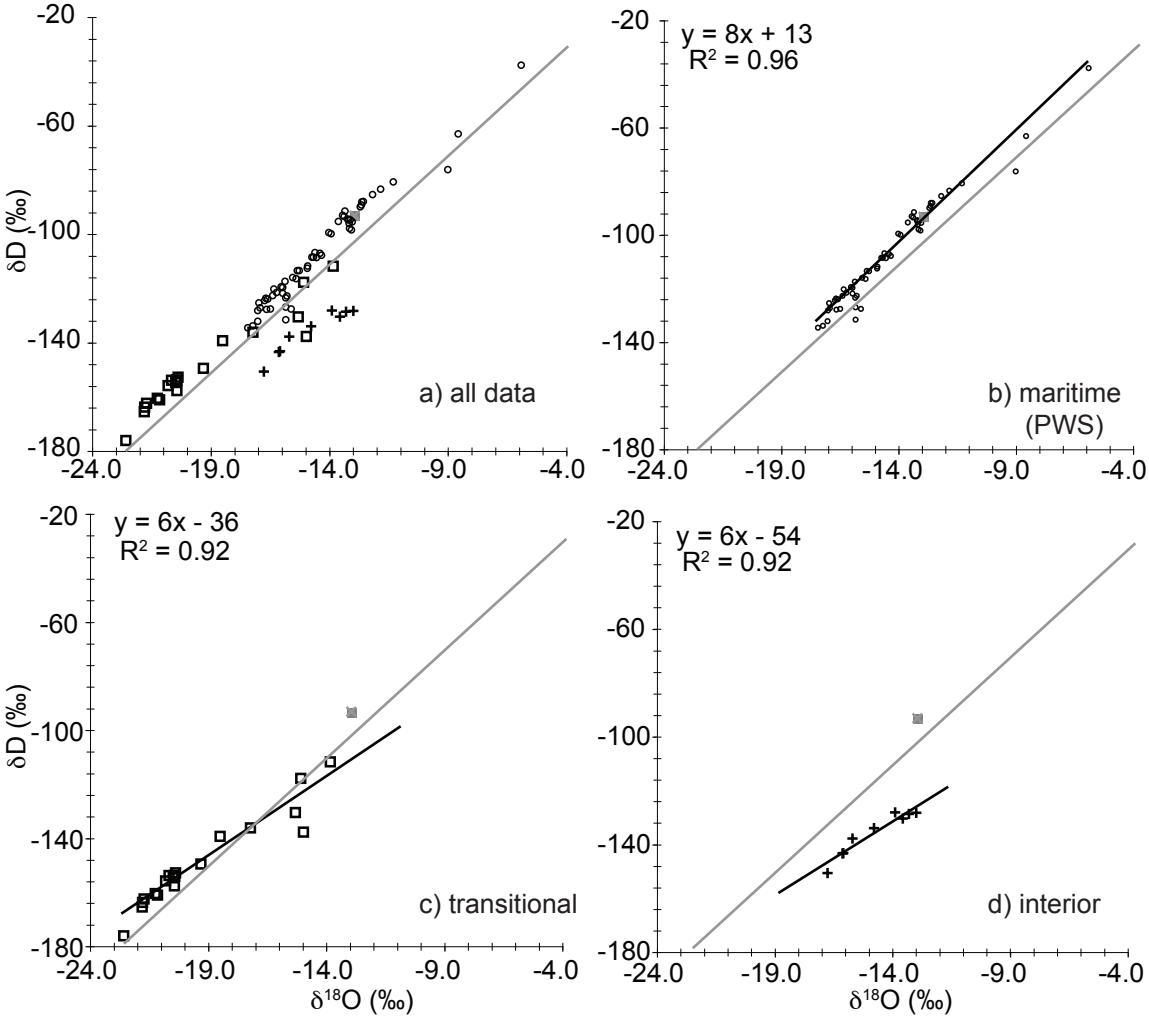

Fig. 9 Water isotope values for samples from 2006 and 2007 lake survey, south Alaska. (a) All data with different symbols indicating different climate regimes, (b,+) PWS, (c,o) transitional, and (d,□) interior samples. Gray line is the global meteoric water line [GMWL; $\delta D = 8\ \delta^{18}O + 10$ (Dansgaard, 1964)] and gray square is Mica Lake surface water. The slope and distance from the GMWL of the least-squares regression for each region provides a measure of evaporative effects. Note that the PWS line is parallel to the GMWL. $\delta^{18}O$ and δD data reported relative to V-SMOW.

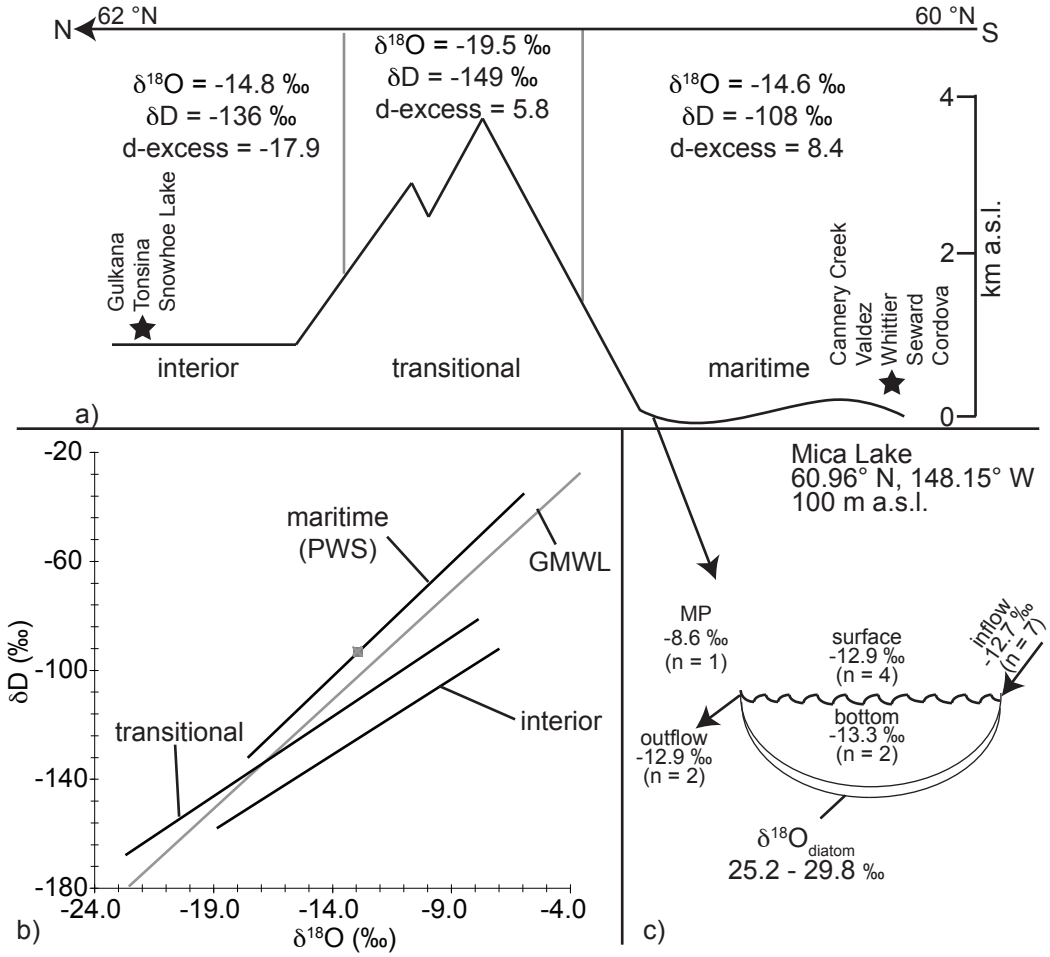

Fig. 10 (a) Summary of south Alaska water isotopes. South-to-north directed arrow indicates general direction of regional moisture transport. Data from (★) climate stations from maritime and interior sites are shown in Fig. 5, and locations are in Fig. 3. $\delta^{18}O$, δD, and d-excess are the averages from all samples collected in each region. Low d-excess values at interior sites reflect the departure of δW values from the GMWL due to evaporation. (b) Summary $\delta^{18}O$ and δD slopes for each region. Gray line is the GMWL and gray square is the surface water at Mica Lake. The lower slope and offset of the interior line from the GMWL confirms evaporative effects, while the parallel and maritime line reflects local precipitation. (c) Water isotope data for samples collected within the Mica Lake watershed. All samples collected during the summer of 2006 and 2007. "MP" refers to Mica Pond (see text for details). $\delta^{18}O$ and δD data reported relative to V-SMOW.

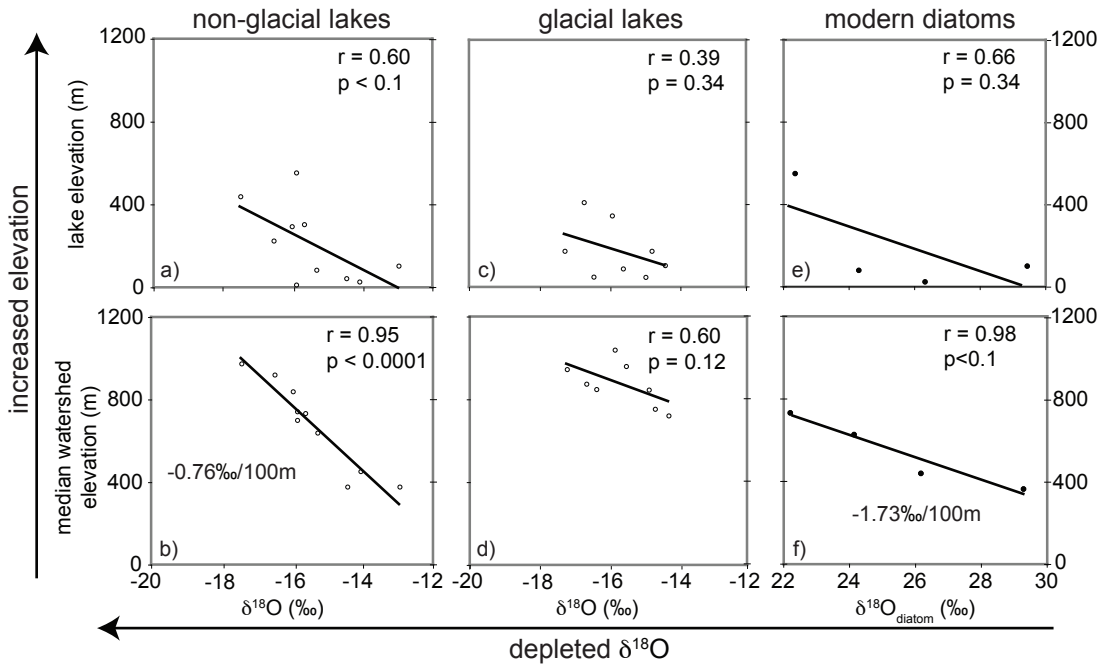

Fig. 11 Lake elevation and median watershed elevation compared with lake water isotope data (δW) for glacial and non-glacial lakes and top-sediment diatoms in the Prince William Sound (PWS). The correlations between δW and median watershed elevation (b, d, f) are stronger and more significant than with lake elevation (a, c, e).

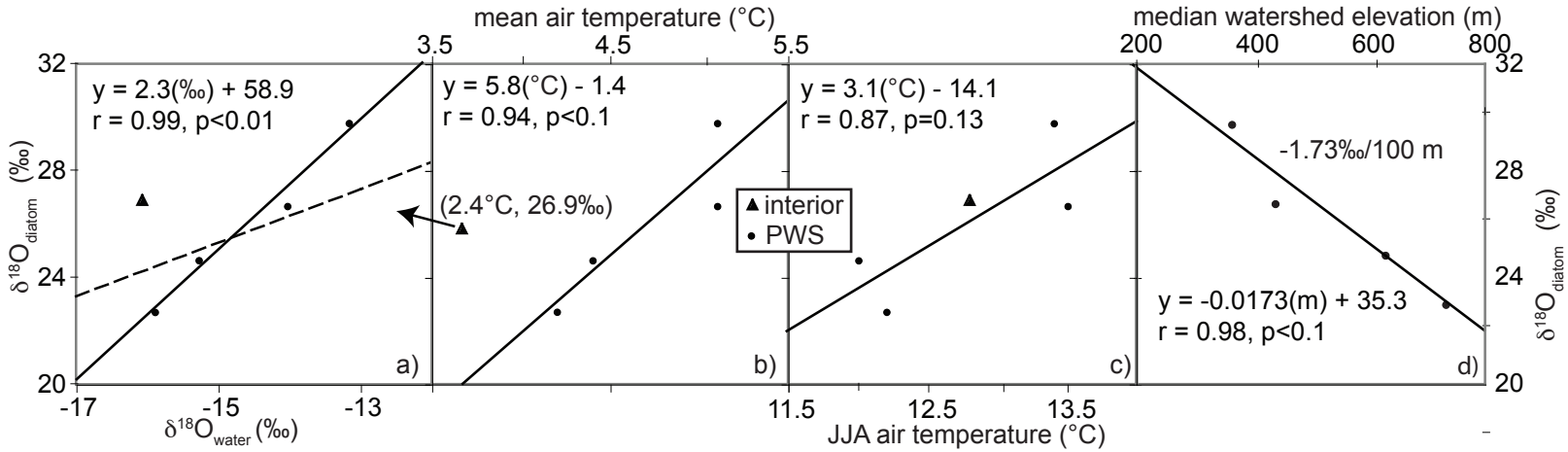

Fig. 12 Relationship between modern $\delta^{18}O_{diatom}$ and a) $\delta^{18}O_{water}$, b) mean annual air temperature (MAT), c) summer air temperature (JJAT), and d) median watershed elevation from four Prince William Sound (PWS) (•) and one interior (▲) lakes. Dashed line in (a) shows the 1:1 fractionation between diatoms and water. Assuming a constant fractionation the observed fractionation factor is, $\alpha = (1000 + \delta^{18}O_{diatom})/(1000 + \delta^{18}O_{water}) = 1.04$.

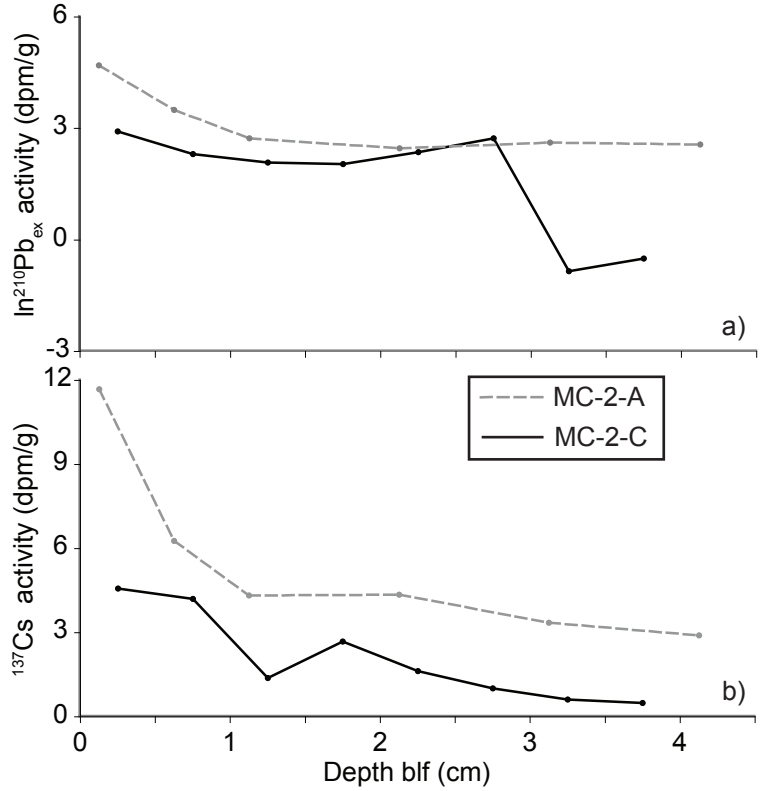

Fig. 13 ^{210}Pb and ^{137}Cs profiles for gravity cores MC-2-A and -C. Data listed in Table 7.

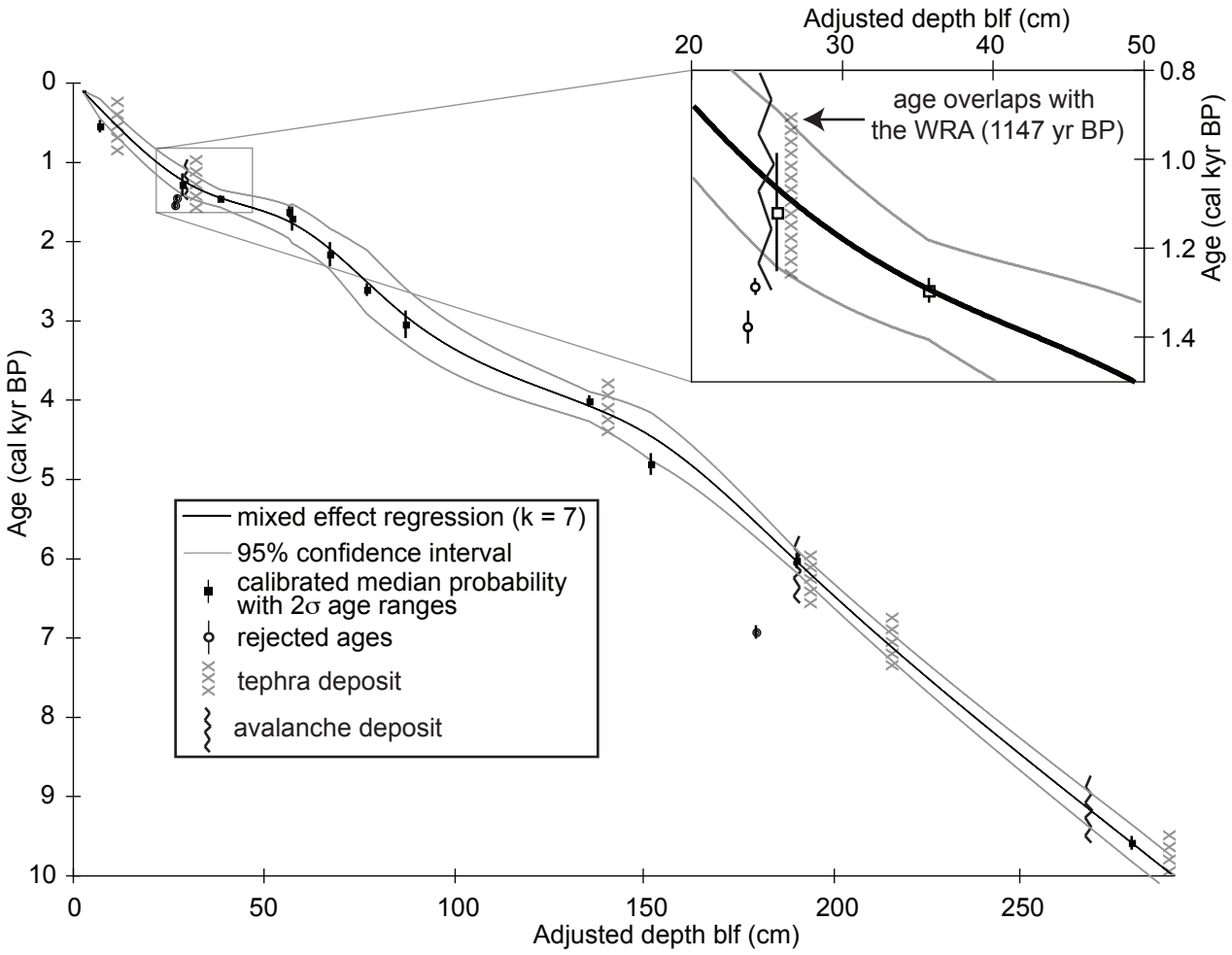

Fig. 14 Spline fit age model (Heegaard et al., 2005) constructed from 13 calibrated ages (see text for details) and the age of the surface sediment (2006). The depths of each dated level was determined after subtracting the cumulative thickness of tephra and avalanche deposits. ^{14}C data listed in Table 8.

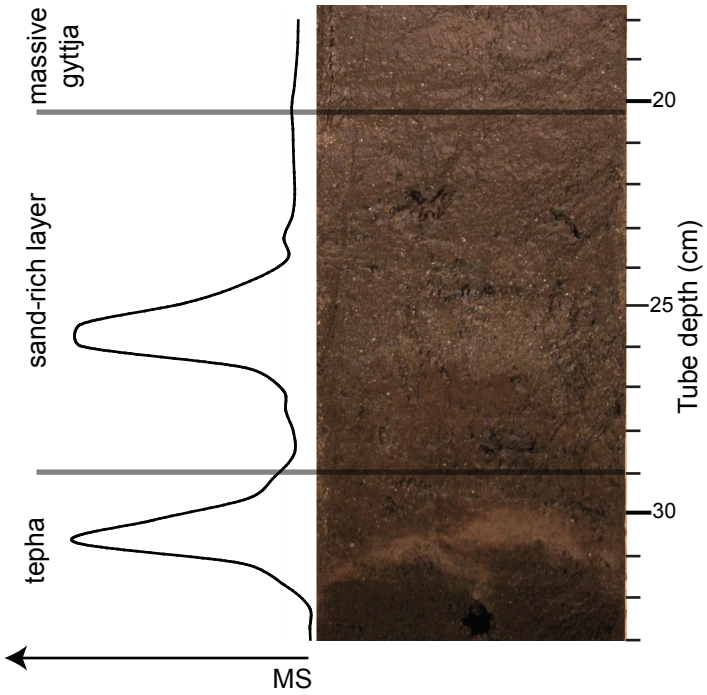

Fig. 15 Photo and magnetic susceptibility (MS) profile of typically lithology of core MC-2. Horizontal bars bound the three distinctive units: tephra, massive gyttja, and sand-rich layers. See text for complete description.

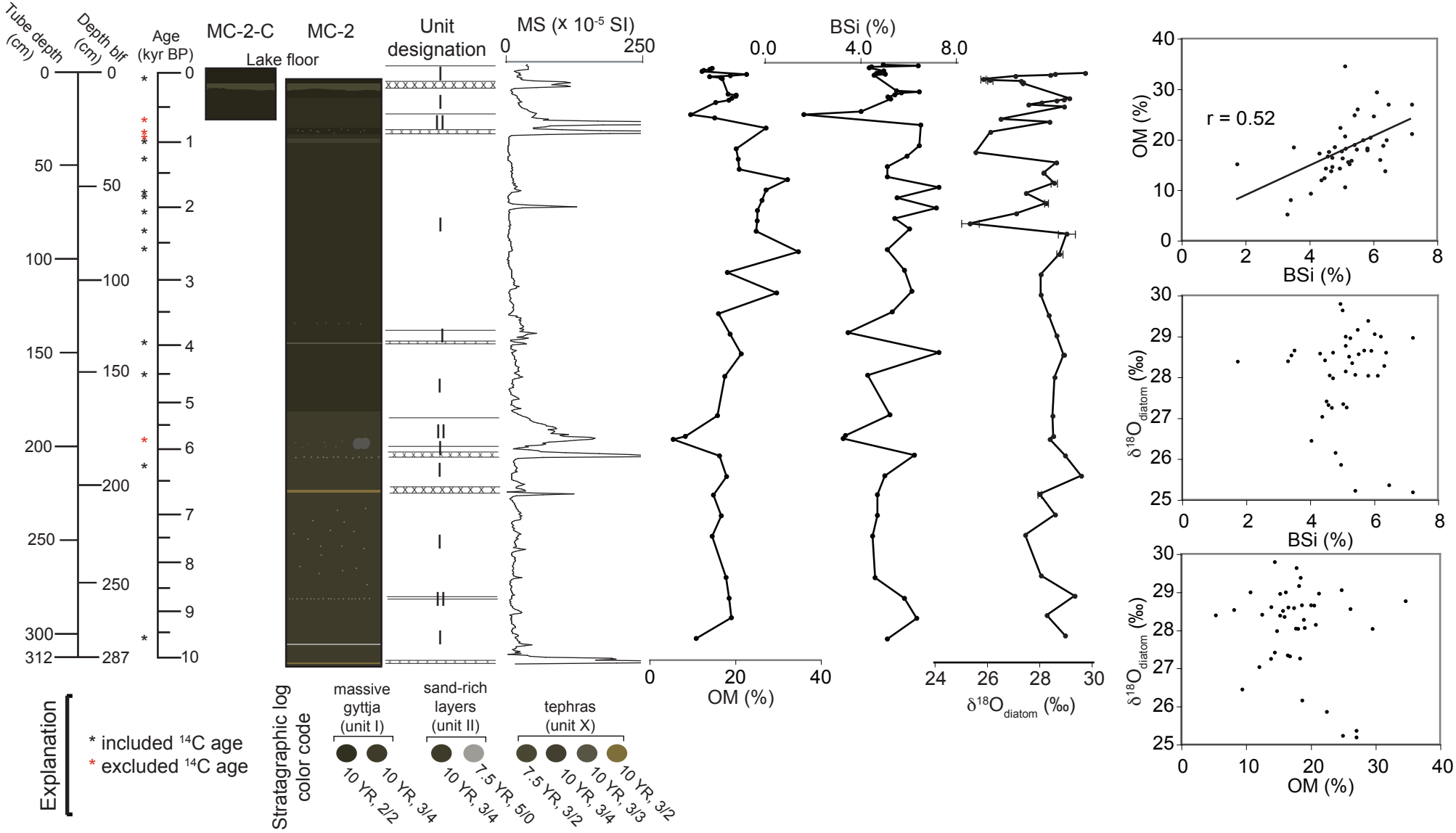

Fig. 16 Geochemical, physical, and chronological summary for core MC-2. The depth below lake floor (blf) is the adjusted of tube depth after adding the thickness of core top that was lost from the percussion core, but recovered in the surface core, and removing the thickness of the tephra and avalanche deposits. Physical and geochemical analyses include magnetic susceptibility (MS), organic matter content (OM), biogenic silica (BSi), and diatom oxygen isotopes ($\delta^{18}O_{diatom}$). Error bars for $\delta^{18}O_{diatom}$ determined from duplicate analyses from 10 horizons and range from 0.0 to 0.5 ‰. Distinct sediment types include: tephra (X), massive gyttja (I), and sand-rich layers (II). $\delta^{18}O_{diatom}$ reported relative to V-SMOW.

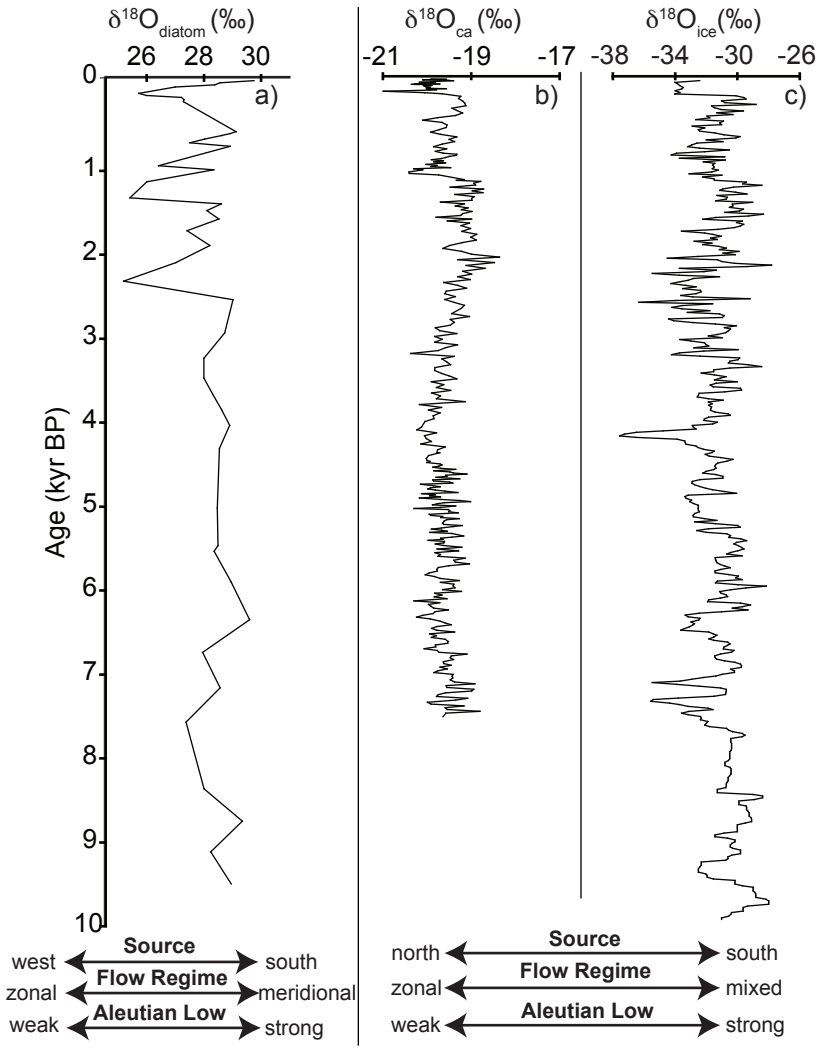

Fig. 17 Oxygen isotope records from (a) Mica Lake diatoms compared to other North Pacific $\delta^{18}O$ records from (b) Jellybean Lake carbonate (Anderson et al., 2005) and (c) Mt. Logan ice cores. The inferred influences of climatic controls discussed in the text are indicated. The climatic interpretations suggested from model simulations by Fisher et al. (2004) explain the variability at Jellybean Lake and Mt. Logan. The Mica Lake and Mt. Logan $\delta^{18}O$ data are reported relative to V-SMOW, whereas Jellybean Lake $\delta^{18}O$ data reported relative to V-PDB.

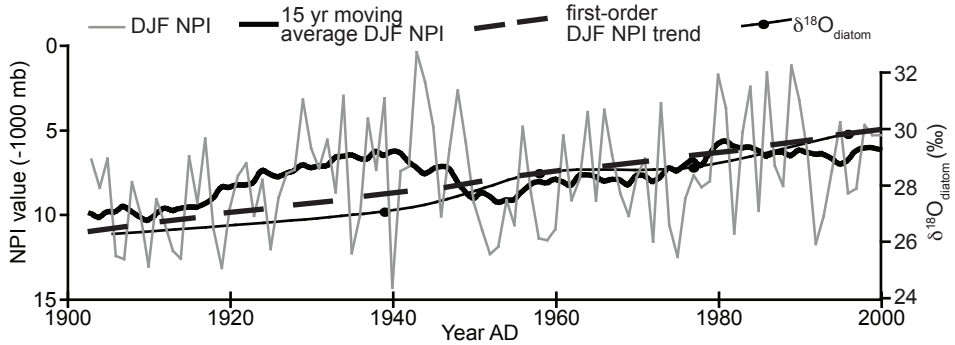

Fig. 18 The 20th century $\delta^{18}O_{diatom}$ values from Mica Lake plotted with the North Pacific Index (NPI). NPI data same as Fig. 2 but with the linear regression (dashed line) fit to emphasize first-order trend. The Mica Lake $\delta^{18}O$ data reported relative to V-SMOW.

Appendix A-1. Magnetic susceptibility data for core MC-2-C

Tube depth	0	20
0.0	36	19
0.5	35	20
1.0	37	22
1.5	38	28
2.0	38	33
2.5	37	36
3.0	20	49
3.5	12	45
4.0	16	44
4.5	23	38
5.0	20	51
5.5	23	71
6.0	16	120
6.5	16	82
7.0	17	72
7.5	20	
8.0	39	
8.5	56	
9.0	67	
9.5	123	
10.0	150	
10.5	133	
11.0	129	
11.5	47	
12.0	18	
12.5	7	
13.0	6	
13.5	5	
14.0	4	
14.5	7	
15.0	7	
15.5	6	
16.0	2	
16.5	5	
17.0	10	
17.5	15	
18.0	17	
18.5	17	
19.0	18	
19.5	18	

Note: The sums of the column and row headings indicate the depth in cm for the magnetic susceptibility readings. Magnetic susceptibility reported in 10^{-6} SI units.

Appendix A-2. Magnetic susceptibility data for core MC-2

Tube depth	0	20	40	60	80	100	120	140	160	180	200	220
0.0	23	49	2	7	1	5	9	6	10	54	10	5
0.5	26	47	4	5	1	7	10	7	11	63	10	8
1.0	24	45	3	3	1	6	10	6	8	70	11	8
1.5	27	52	0	2	1	6	10	6	11	72	11	11
2.0	48	75	-1	1	0	6	9	8	4	83	13	12
2.5	106	66	-1	-1	1	7	8	15	3	89	14	12
3.0	115	167	1	-1	1	7	6	12	3	91	15	14
3.5	94	341	1	1	1	6	1	7	3	75	16	13
4.0	82	629	3	1	2	6	2	8	5	86	15	15
4.5	109	627	6	1	4	7	16	9	5	87	16	15
5.0	115	178	7	0	1	10	16	10	5	84	14	17
5.5	53	79	7	4	5	10	23	12	8	81	17	19
6.0	12	69	6	9	5	11	23	12	12	112	10	19
6.5	8	48	7	34	5	11	21	13	16	98	6	23
7.0	6	48	8	82	5	10	23	12	19	105	6	25
7.5	8	100	7	128	5	12	22	15	21	153	7	20
8.0	8	172	8	27	5	11	22	15	11	163	6	21
8.5	7	430	8	13	6	13	24	14	7	156	6	25
9.0	9	648	5	4	6	20	23	13	6	126	7	22
9.5	14	189	7	2	6	15	27	13	6	106	7	23
10.0	17	73	8	2	8	15	29	14	6	77	11	23
10.5	17	6	7	3	6	7	28	15	6	65	17	22
11.0	17	4	7	2	1	4	22	20	10	69	20	12
11.5	20	2	6	2	1	4	29	18	13	63	24	8
12.0	21	2	7	2	2	2	27	19	17	32	31	7
12.5	23	2	9	1	1	2	23	19	24	38	25	8
13.0	25	2	10	2	1	3	38	20	12	20	18	9
13.5	19	2	9	2	1	3	52	16	7	9	15	10
14.0	21	2	10	2	0	3	35	12	9	40	15	9
14.5	21	2	10	2	0	3	33	16	12	57	25	9
15.0	22	1	8	3	-1	5	29	20	17	62	31	12
15.5	25	2	13	4	1	5	17	20	19	108	33	11
16.0	26	1	10	4	0	3	37	28	24	170	-2	11
16.5	30	1	13	4	1	3	27	21	27	229	41	14
17.0	36	1	17	5	0	5	5	12	33	261	123	17
17.5	37	1	14	2	1	7	5	8	38	303	64	20
18.0	41	0	13	4	1	9	13	8	42	64	15	25
18.5	47	0	15	3	1	10	29	8	42	19	8	18
19.0	54	-1	24	3	3	11	35	8	45	14	6	19
19.5	50	2	19	1	4	10	9	7	47	11	4	17

Note: The sums of the column and row headings indicate the depth in cm for the magnetic susceptibility readings. Magnetic susceptibility reported in 10^{-6} SI units.

Appendix A-2. (continued)

Tube depth	240	260	280	300
0.0	16	16	4	25
0.5	18	25	6	-1
1.0	15	10	6	36
1.5	14	7	5	41
2.0	12	5	6	70
2.5	12	4	5	192
3.0	13	5	6	200
3.5	14	3	7	164
4.0	15	4	7	299
4.5	16	5	7	477
5.0	10	7	10	203
5.5	20	7	12	14
6.0	32	5	13	
6.5	22	6	13	
7.0	13	6	9	
7.5	8	8	8	
8.0	6	7	6	
8.5	6	8	7	
9.0	6	8	9	
9.5	9	11	8	
10.0	12	7	15	
10.5	13	6	18	
11.0	12	6	18	
11.5	14	6	14	
12.0	14	3	13	
12.5	12	3	18	
13.0	10	5	17	
13.5	11	4	19	
14.0	10	5	22	
14.5	9	6	21	
15.0	9	6	26	
15.5	10	9	45	
16.0	10	8	31	
16.5	9	11	15	
17.0	8	13	15	
17.5	10	18	13	
18.0	10	22	9	
18.5	8	26	12	
19.0	10	24	22	
19.5	11	10	14	

Note: The sums of the column and row headings indicate the depth in cm for the magnetic susceptibility readings. Magnetic susceptibility reported in 10^{-6} SI units.

Appendix B-1. Biogenic silica (BSi), organic matter (OM), and diatom oxygen isotope ($\delta^{18}O_{diatom}$) data for core MC-2

Depth	BSi	OM	$\delta^{18}O_{diatom}$ (‰)		
(blf)	(%)	(%)	run 1	run 2	AVG
0.25	4.9	14			29.8
0.75	6.4	14			28.6
1.25	4.5	12			28.4
1.75	4.4	12			27.0
3.25	5.0	22	25.9	25.7	25.8
3.75	4.8	19	26.2	25.9	26.0
4.25	4.7	14			27.3
4.75	5.0	16			27.4
5.25	4.6	17			27.3
12.75	5.5	18			29.2
13.25	6.4	20			29.0
13.75	5.7	20			28.7
14.75	5.4	19			28.1
15.75	5.1	18			27.6
16.75	5.2	15			29.0
22.75	4.0	9			26.5
24.25	1.7	15			28.4
29.25	6.5	27			26.1
39.25	6.4	20			25.5
44.25	5.9	20			28.7
49.25	5.1	21	28.2	28.2	28.2
54.25	5.1	32	28.7	28.5	28.6
59.25	7.2	27			27.5
64.25	5.5	26	28.2	28.3	28.3
69.25	7.1	25			27.1
74.25	5.4	25	25.6	24.9	25.2
79.25	6.0	25	29.4	28.7	29.1
89.25	5.1	35	28.9	28.7	28.8
99.25	5.8	18			28.0
109.25	6.1	29			28.0
119.25	5.3	16			28.4
129.25	3.5	19			28.7
138.75	7.2	21	29.0	28.9	29.0
149.75	4.3	17			28.6
168.75	5.2	16			28.5
178.75	3.4	8			28.5
180.25	3.3	5			28.4
188.25	6.2	16			29.0
198.25	5.0	18			29.6
207.25	4.7	15	28.0	28.0	28.0
217.25	4.7	16			28.6
227.25	4.5	14			27.4
247.25	4.6	18			28.1
257.25	5.8	18			29.4
266.75	6.3	19			28.3
276.75	5.1	11			29.0

Note: Centered depth of 0.5-cm-thick samples. Isotope values reported vs. V-SMOW.